

DRAFT
September 26, 2007

Report of the NSLS-II Stability Task Force

Table of Contents

1. Executive Summary
2. General NSLS-II Beamline Stability Guidelines
3. Stability Requirements for NSLS-II Beamlines
4. Conventional Construction
5. Mechanical Systems
6. Orbit Feedback
7. Electrical Systems
8. RF System

1. Executive Summary

The NSLS-II has been designed to provide ultra high-brightness x-ray sources. The storage ring is comprised of 30 double-bend-achromatic cells and has 15 superperiods. The insertion device straight sections have lengths 6.6m (low betax and betay) and 9.3m (high betax and low betay). The lattice without insertion devices has 2nm-horizontal emittance. Damping wigglers will be used to reduce the horizontal emittance below 1nm. The vertical emittance is chosen to be the diffraction limit for 1 Angstrom radiation, i.e. 8pm.

To realize the benefits of the high brightness and small beam sizes of NSLS-II, it is essential that the photon beams are exceedingly stable in position and angle. For timing experiments, it is also necessary that the arrival-time jitter of the bunch be small. We shall require transverse beam motion to be less than 10% of beam size or angular spread, and longitudinal beam motion to be less than 5% of equilibrium bunch duration. We also require that the transverse beam dimensions not vary by more than 10%. Ideally, the temporal, spatial and angular stability of the electron beam should be maintained for at least the duration of spectral scans, which typically run from a few ms to a few hours.

$$\begin{aligned}\Delta x &< 0.1\sqrt{\beta_x \epsilon_x + \eta^2 \sigma_p^2} & \Delta x' &< 0.1\sqrt{\epsilon_x / \beta_x + \eta'^2 \sigma_p^2} \\ \Delta y &< 0.1\sqrt{\beta_y \epsilon_y} & \Delta y' &< 0.1\sqrt{\epsilon_y / \beta_y} \\ \Delta t &< 0.05 \sigma_t & \Delta p / p &< 0.05 \sigma_p \\ \Delta \sigma_{x,y} &< 0.1 \sigma_{x,y}\end{aligned}$$

Our philosophy is to follow best engineering practices to optimize the passive stability of the facility within reasonable cost. Active orbit feedback will be used to achieve the very high level of stability required by the users. Feed forward on skew quadrupoles will be used to stabilize vertical beam size while changing insertion device gaps.

We shall employ top-off injection which produces stable heating from the electron beam. At a particular location in the storage ring tunnel the temperature will be regulated to $\pm 0.1^\circ C$. On the experimental floor temperature regulation to $\pm 0.5^\circ C$ will be sufficient. Temperatures of the experimental beamlines and end-stations can be held to tighter tolerance as required by the individual research programs.

Great care must be taken in the design to isolate the concrete floor from roof supports and from vibrating mechanical equipment. The goal is to keep vertical floor motion below 25nm in the frequency bandwidth 4-50 Hz, where the motion is expected to be uncorrelated. The magnets will be placed on specially designed girders which have no resonance below 50 Hz, so there will be negligible amplification of vibration amplitude from the floor to the top of the girder for frequency below 50 Hz. Floor motion falls off fast at higher frequency ($\sim 1/\omega^4$). Even if there is some amplification by the girder above 50 Hz the effect on the electron beam is expected to be small. The floor motion at frequencies below 4 Hz can be significantly larger. The effect on the electron beam of vibrations with frequency below 4 Hz is reduced since the associated wavelength is long and major portions of the storage ring containing many girders move together. However, we can expect significant motion of the electron beam with frequency below 4 Hz that will need to be reduced by feedback.

There is an amplification factor between quadrupole displacement and the movement of the electron beam. Quadrupoles vibrating randomly and independently with rms amplitude of 25 nm will generate electron orbit motion with rms amplitude ~ 350 nm at a location with unit beta function. Since the quadrupoles on a girder move in a correlated manner, random and independent motion of the girders with rms amplitude of 25 nm will generate less motion of the orbit (~ 120 nm at a location with unit beta function) than would independent motion of the quadrupoles.

Dipole, quadrupole and sextupole power supply stability requirements are within standard achievable limits (< 50 ppm for dipoles and < 100 ppm for multipoles). With a well-corrected orbit having less than $100 \mu m$ displacement in the quadrupole magnets, the quadrupole power supply variation will produce $< 0.2 \mu m$ motion of the electron beam. Variation in the dipole field ($\Delta B / B$) will cause a motion of the electron beam, $\eta(\Delta B / B)$, where η is the storage ring dispersion. At a location with $\eta \sim 0.1 m$, the horizontal motion of the electron beam will be $5 \mu m$. Since the fractional energy spread $\sigma_p \sim 10^{-3}$, the beam size at this location is $> 100 \mu m$. The variation in the dipole field will result in a variation in the average electron energy which will result in an arrival-time jitter of $< 5\%$ of the equilibrium bunch duration.

The tightest orbit tolerance is required at the undulator sources located in the 6.6m-long low-beta insertions. The rms vertical beam size is $3 \mu m$ at these locations and the rms vertical angular spread is $3 \mu rad$. Therefore, our goal is to hold the electron orbit constant to $\pm 0.3 \mu m$ at the beam position monitors (BPMs), separated by ~ 5 m, bounding the straight section. A temperature variation of $\pm 0.1^\circ C$ will produce $\pm 1.1 \mu m$ motion of the BPM if it is supported from the floor by 1 m of structural steel. Therefore, the BPMs bounding the undulator straights must be supported by stands made from materials with low coefficient of thermal expansion, or by thermally stabilized steel stands. Our goal is to have the thermal motion no greater than $\pm 0.1 \mu m$ vertically and $\pm 1 \mu m$ horizontally. The other BPMs around the ring will be incorporated into the aluminum chamber. Consideration is being given to the possibility of constraining them with invar, so that they also can be held fixed vertically to better than $0.2 \mu m$.

The design of the RF BPMs uses the Libera digital processors. For the BPMs bounding the low-beta insertions, our goal is to achieve a measurement precision of $0.1 \mu m$ within 100 Hz bandwidth. This is about a factor of 2 better than the present state-of-the art. Although early operation of the orbit feedback system would be based on the RF BPMs, the system architecture will be designed to include x-ray BPMs on the user beamlines. We plan to implement the Decker distortion in order to simplify the radiation background for the x-ray BPMs on insertion device beamlines

The quadrupoles and sextupoles will be aligned on girders to better than $50 \mu m$, and girders will be aligned relative to each other to better than $100 \mu m$. Beam-based alignment will be used to calibrate the BPMs relative to the quadrupoles and sextupoles. The orbit correction system contains 6 correction magnets and 7 BPMs per period. It has the capability of correcting the misalignment expected during first commissioning of the

storage ring as well as for the long-term settlement of the concrete floor (estimated to be 10 $\mu\text{m}/10 \text{ m/year}$).

The orbit feedback system uses a subset of 4 BPMs and 4 correction dipoles per cell ($\times 30$). These correction dipoles are located over stainless steel chambers so the feedback correction bandwidth is greater than 60 Hz. The correction dipoles will be driven by the sum of two signals, one slow with the ability to drive the power supply to the maximum strength of 800 μrad and the other fast with the strength falling off at higher frequency. The resolution of the last bit is $<0.01 \mu\text{rad}$ and the noise level is $<0.003 \mu\text{rad}$. This corresponds to $<4\text{ppm}$ of 800 μrad .

Beam size stabilization is also of great importance. Beam size correction for gap change in an insertion device requires feed forward using skew quadrupoles near the insertion device. These skew correctors should have high bandwidth commensurate with gap-change speeds, especially for EPU's. We also plan to feed forward using dipole correctors to reduce orbit perturbation during insertion device gap changes.

2. General NSLS-II Beamline Stability Guidelines

The electron beam sizes and angular divergences for selected NSLS-II sources, including insertion device straight sections, bending magnets, and three-pole wigglers, is provided in Table 2.1.

Table 2.1. Electron Beam Sizes and Divergences for selected NSLS-II sources

Type of source	5 m straight section	8 m straight section	Bend magnet *	1T three-pole wiggler
σ_x [μm]	38.5	99.5	44.2 (35.4-122)	136
σ_x' [μrad]	14.2	5.48	63.1 (28.9-101)	14.0
σ_y [μm]	3.05	5.51	15.7	15.7
σ_y' [μrad]	3.22	1.78	0.63	0.62

The size and angular divergence of photon beams from NSLS-II insertion devices, as a function of photon energy, are shown in Figs. 2.1 and 2.2. Both the source size and source divergence values diverge from the diffraction-limited value above ~ 1 keV photon energy, owing to the quadrature contribution of the electron beam size and angular divergence. In general, the beamlines which provide the most stringent requirements on beam stability are those that accept only the diffraction-limited portion of the photon beams. Above ~ 1 keV, overfilling of a diffraction-limited beamline acceptance (both space and angle) provides a degree of tolerance to beam motion. Below ~ 1 keV, the photon beam is diffraction-limited in the vertical and there is less fractional tolerance to beam motion in that direction. The absolute stability requirements on the electron beam should be determined at high photon energy, where the diffraction-limited photon phase space is smallest. We propose the following electron beam stability requirements: spatial stability = 10% of U19 CPMU (in 5m ID straight) photon beam size at high energy (50 keV), angular = 10% of U19 divergence at high energy (50 keV):

- vert. position: 10% of 3 micron = 0.3 micron
- vert. angle: 10% of 7 microradian = 0.7 microradian
- horiz. position: 10% of 40 micron = 4.0 micron
- horiz. angle: 10% of 15 microradian = 1.5 microradian

The corresponding fractions of the electron beam size in the 5m ID straight sections are:

- vertical position: 0.3 micron / 3 micron = 10%
- vertical angle: 0.7 microradian / 3 microradian = 24%
- horizontal position: 4.0 micron / 40 micron = 10%
- horizontal angle: 1.5 microradian / 15 microradian = 10%

Since some beamline experiments may need greater stability than the values quoted above, consider a "stretch" goal which is 3 times tighter, i.e.

- vert. position: 0.1 micron / 3 micron = 3% of vert. ebeam size
- vert. angle: 0.2 microradian / 3 microradian = 7% of vert. ebeam divergence
- horiz. position: 1.3 micron / 40 micron = 3% of horiz. ebeam size
- horiz. angle: 0.5 microradian / 15 microradian = 3% of horiz. ebeam divergence

Time dependence: Ideally, the spatial and angular stability of the electron beam should be maintained for at least the duration of spectral scans, which typically run from a few ms to a few hours.

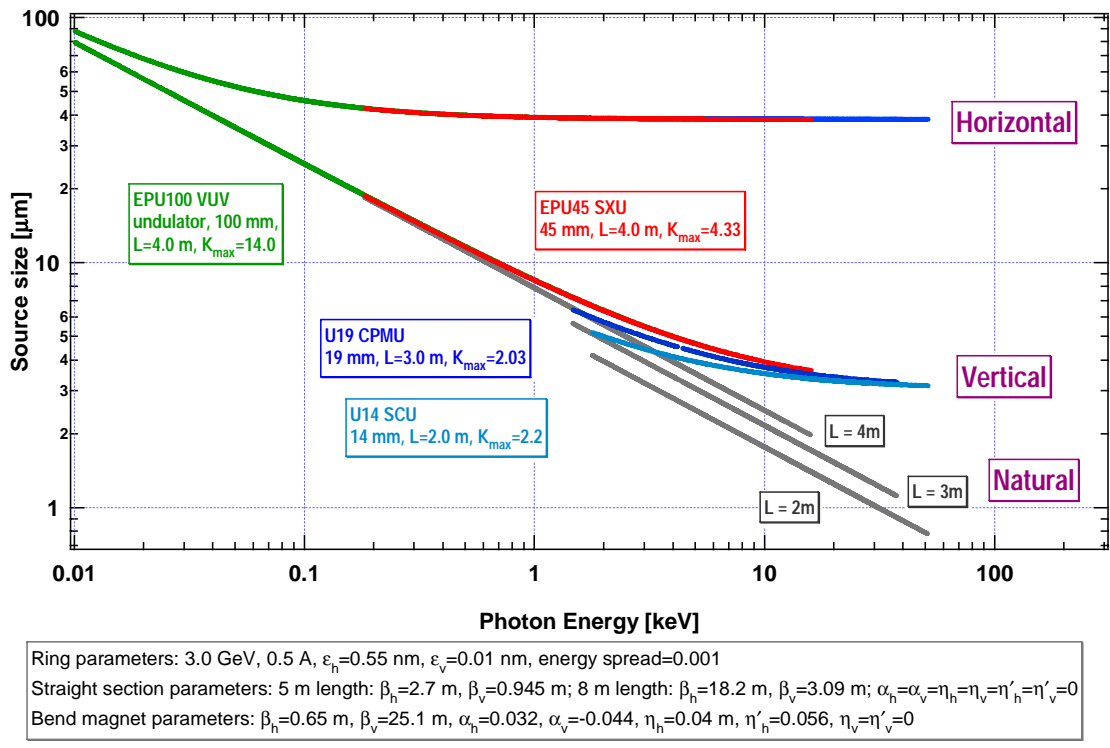


Figure 2.1: Source Size vs Photon Energy

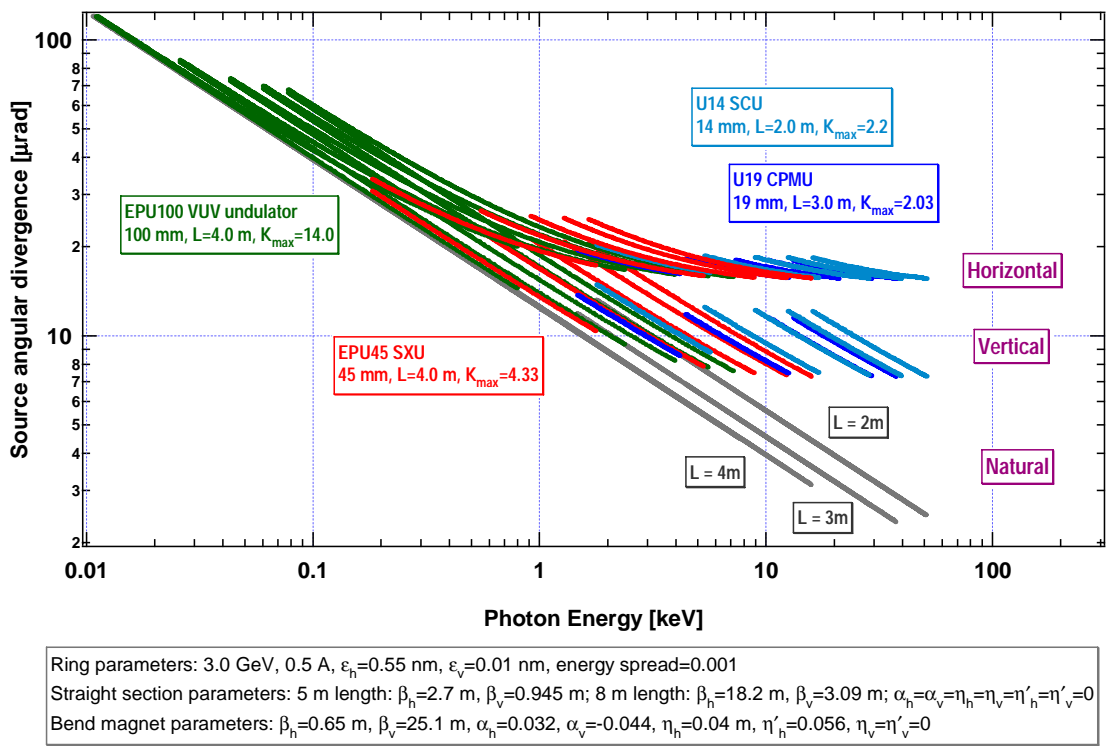


Figure 2.2 : Source Angular Divergence vs Photon Energy

3. Stability Requirements for NSLS-II Beamlines

The experimental programs that will be represented at NSLS-II beamlines have a range of stability requirements. These are elaborated on in the sections which follow. In the table presented here (following page), we summarize the most stringent of these requirements, for each of the major programs, in terms of the beam position centroid and width stability requirements and the beam angle centroid and width stability requirements, in both the horizontal and vertical directions, as well as the driving reason for each of these. We find, interestingly, that some of the more conventional experimental programs have demanding requirements, in order to satisfy their state-of-the-art science objectives for a cutting-edge source like NSLS-II. We also find that beam position and angle motions could not only have impact on the definitions of the resolution functions (for position, angle, and wavelength) which the beamline optical systems deliver, but also on the intensity throughput which is just as important, for many of these programs, to keep stable. These issues are treated individually for each program. Finally, for some programs, the table below identifies the stability requirements as being in need of further study (or, for those table cells for which entries are missing, the relevant information is not yet at hand). It's already clear, for some programs, that the requirements have to be very stringent (e.g. for scanning transmission x-ray microscopy).

3.1 Stability Requirements for Inelastic X-Ray Scattering Beamlines

All of the concepts which have been investigated for delivering very fine energy resolution x-ray beams involve the use of multiple Bragg reflection crystal optics, often involving asymmetric Bragg reflections and sometimes utilizing back-reflection. These features are all in the makeup of schemes which have been studied already, or are under active investigation, whose objective is to deliver 0.1 meV energy resolution. These have in common that a very narrow vertical angular fan of the beam emerging from the source is employed. For an instrument which delivers 0.1 meV energy resolution, the peak of the spectral distribution function after monochromator needs to be stable to better than 0.01 meV. It is estimated that this would require stability of the incident beam direction (beam angle) to 10% of the vertical beam opening angle. In the horizontal direction, the requirements are not nearly as stringent (in an absolute sense).

3.2 Stability Requirements for Infrared Beamlines

Motion of the beam or optical components, whether position or angle, affects the signal reaching the detector at the endstation of an infrared beamline. Typical focal lengths for collecting and transporting beam are on the order of 1 meter, so a 1 μm shift in position is equivalent to a 1 μrad angular displacement. In general, the optical systems are somewhat more tolerant to angular deviations so for simplicity we state requirements only for position.

We note that some near- and mid-infrared detectors are highly sensitive and would be affected by extremely small beam displacements. However, only a few measurements might exploit this sensitivity, so our stability requirements are based on calculated S/N tolerances as well as practical experience.

Practical experience at the NSLS VUV ring suggests that a 10-fold reduction in beam motion would be beneficial for nearly all measurements, and a 100-fold improvement would reduce noise to a level where its contribution is comparable to other typical noise sources. Measurements of the apparent beam motion at an NSLS IR endstation show displacements up to 50 μm when

Program	Vertical Position Stability			Vertical Angle Stability			Horizontal Position Stability			Horizontal Angle Stability			Radiation Source(s)	Frequency or Time Range					
	Centroid (μm unless otherwise noted)	Width (μm unless otherwise noted)	Driver	Centroid (μrad unless otherwise noted)	Width (μrad unless otherwise noted)	Driver	Centroid (μm unless otherwise noted)	Width (μm unless otherwise noted)	Driver	Centroid (μrad unless otherwise noted)	Width (μrad unless otherwise noted)	Driver							
Inelastic x-ray scattering	10% of beam size			10% of opening angle		energy stability	10% of beam size			10% of opening angle			CPMU or SCU	minutes to ~4 hours					
Infrared		15% of sigma	intensity stability		35% of sigma	intensity stability		25% of sigma	intensity stability		65% of sigma	intensity stability	Dipole	few Hz to 20 kHz					
Macromolecular crystallography		1	sample size		1	energy stability		1	1	sample size and diffracted beam intensity (from sample) stability		4	4	intensity stability	CPMU or SCU	few msec to ~2 hours			
Nano-focusing/probe	10% of beam size	1% of beam size	spot size and 1% intensity stability	10% of opening angle	10% of opening angle		10% of beam size	1% of beam size	spot size and 1% intensity stability	10% of opening angle	10% of opening angle		CPMU or SCU	up to 1-2 hours					
Powder diffraction		10	detector spatial resolution		1	energy stability		10	detector spatial resolution	not applicable			DW or 3PW						
Small angle x-ray scattering		20	~7% of sigma	1% intensity stability		8	not as sensitive	1% intensity stability		8	~2% of sigma	1% intensity stability	3	~3% of sigma	1% intensity stability	CPMU or SCU	few msec to ~2 hours		
Soft x-ray	10% of beam size		energy stability	10% of opening angle			10% of beam size		spot size on sample	10% of opening angle			Undulator or Dipole	few msec to hours					
High-energy x-rays		50	50	sample size		10	10	energy stability		50	not applicable	sample size	not applicable	not applicable	not applicable	SCW	few msec to hours		
X-ray absorption spectroscopy	10% of beam size	10% of beam size	beam position on sample		1	10% of opening angle	energy stability	10% of beam size	10% of beam size	beam position on sample	10% of opening angle	10% of opening angle	beam position on sample	DW or 3PW or Dipole	100 msec to 10 hours				
X-ray magnetic circular dichroism	Needs further study			Needs further study				Needs further study			Needs further study			EPU's					
X-ray photon correlation spectroscopy		0.2				0.1							1		CPMU or SCU	100 μsec to ~2 hours			
Scanning transmission x-ray microscopy		0.03	0.03	0.01% intensity stability		0.006	0.006	0.01% intensity stability		8	0.1	0.1	0.01% intensity stability		0.015	0.015	0.01% intensity stability	Undulator	10 μsec to 100 sec

measured at a 1 meter focus (i.e., 50 μrad). This defines a stability goal of 0.5 μm (100X improvement).

Similarly, the resolution of spectrometer digitizers suggests a S/N goal of at least 300:1. This sets a limit on beam position fluctuations at 0.4% of the RMS effective beam size under typical conditions. The effective source size at the shortest wavelength of interest (2 μm) is about 200 μm , defining an absolute goal/requirement of ~ 1 μm stability. This value is comparable to that estimated from practical experience, so we use this value (1 μm) as our stability goal.

Though beam motion at any frequency degrades the effective brightness, infrared measurements are directly sensitive to beam motion from a few Hz up to 20 kHz. The 1 μm stability goal applies to this entire frequency range.

Noise studies at the NSLS VUV ring suggest a mixture of electrical and mechanical sources. Mechanical noise (fans, water pumps) dominates at frequencies immediately below 60 Hz. Electrical noise includes 60 Hz and harmonics (power supplies for magnets) and higher harmonics to a few kHz (phase noise from RF system electronics).

3.3 Stability Requirements for Macromolecular Crystallography Beamlines

Mostly as a result of sample size, and the emerging preference to deliver very small beams to the experiment, a position stability of ~ 1 μm or better (horizontally and vertically), at the sample, is needed, and in any case not more than 5% of the sample size which might be smaller than 20 μm . Note that this translates directly into source stability if the beamline optics focus at 1:1 magnification. As far as angular stability is concerned, it should be within 5% of a sample's rocking curve (which might be as narrow as ~ 100 μrad wide) in the vertical direction, as well as within 5% of the angular separation between adjacent Bragg reflections that need to be distinguished (this separation can be ~ 1 mrad) in the horizontal and vertical directions. But because the beam-defining aperture, before the monochromator, subtends 50 (80) μrad in the vertical (horizontal) direction, and because the intensity delivered through this aperture must be stable to within 5% or less (see below), these requirements in composite argue for an angular stability of ~ 2 μrad vertically and ~ 4 μrad horizontally. Closer inspection shows that, for the purpose of wavelength stability as required for high-resolution anomalous diffraction measurements, an angular stability in the vertical direction of ~ 1 μrad in the beamline is called for. This is needed in order to preserve the wavelength definition, using a Si(111) monochromator, to within 4% of the width of the very sharp selenium K edge, where measurements are often made. Strictly speaking, this criterion may be relaxed because a beam defining aperture is used before the monochromator, however an angular instability in this circumstance will become an intensity instability. The intensity delivered to the sample should not vary by more than 1% from frame to frame (which might have an exposure time of a few milliseconds) through the entire duration of a full data set from a sample (which might last for as much as 2 hours). For experiments performed at these beamlines, it is of utmost importance that the final beam conditioning components (apertures and perhaps a final focusing element) be mounted on the same support as the diffractometer holding the sample. For micro-diffraction applications in particular, the total distance spanning these components may be as little as several centimeters. Instruments that meet these needs either already exist or are under development.

3.4 Stability Requirements for Nano-Focusing Beamlines

From the point of view of nano-focusing, a 10% criterion on the position of the beam seems to be an effective stability criterion. A 10% positional instability contributes negligibly to the broadening of the effective spot size. One can imagine that typical images will be generated that will take 1 hour or so. Images that take 10 hours to generate will be considered as experiments that cannot be done, and so eventually all the experiments that will be considered doable will have scans that take at most 1 or 2 hours. Within such a scan it will be important to keep the beam stable to 10%. Typically then after a scan, calibration markers can be used to relocate the beam, and then for the next scan one has to assume that the beam is stable. The maximum overhead one can allow for checking on the beam position is 10% of the typical scan time so that would be of order 10 minutes.

A 10% beam positional stability also translates into less than 1% fluctuations in signal intensity, and this is also acceptable.

3.5 Stability Requirements for Powder Diffraction Beamlines

Powder diffraction will probably operate in two modes, area detector and crystal analyzer. The crystal analyzer mode is the most demanding in terms of angular stability, since it aims to provide high d-spacing resolution and precision. Area detector mode is primarily affected by position stability. Both are sensitive to beam energy changes.

In crystal analyzer mode, the critical thing is angular stability. A typical powder peak width using an analyzer crystal is in the range $0.001 - 0.01^\circ$ at 17 keV, depending on the sample quality. 0.001° is unusually good. Let us take 0.005° as typical. Then the beam stability should be 10% of that, i.e. 0.0005° , or 8 μrad .

A related concern is the energy stability, since energy maps directly to d-spacing in a diffraction experiment. Using Si(111), its intrinsic energy resolution is $\sim 10^{-4}$, which sets a limit on what we can achieve with a sample. If we assume we can find centroids to a few percent of that, we end up with an energy stability requirement of at least 10^{-5} . This maps to an angular stability of 1 or 2 μrad (Si(111) at 17 keV has a Darwin width of 15 μrad), and a monochromator temperature stability of better than 10 K.

All of the above arguments are directed at the plane of diffraction, i.e. vertical.

Area detector measurements are typically 10 times or more lower resolution than this, so are not the limiting case for angular stability. In contrast to the crystal analyzer mode, position stability is important, since position is used as an angle analog. If we assume a focused beamline with a focal spot of 100 μm and a detector with similar spatial resolution, then using the 10% rule, beam position stability should be at the 10 μm level. Similar arguments apply to the energy stability.

In this case, the spatial stability requirements are in both horizontal and vertical directions.

3.6 Stability Requirements for SAXS Beamlines

1. SAXS and USAXS on bulk samples: beam intensity (time) stability

For many small angle x-ray scattering (SAXS) measurements, beam intensity stability is important since the scattering patterns from the sample itself and the sample holder that contributes to the background scattering are measured separately. Since the background scattering sometimes is comparable in magnitude as sample scattering, high beam intensity stability (<1%) is desirable for the purpose of accurate background subtraction. Positional stability is usually not a concern for these measurements.

In a SAXS instrument, the beam size and direction are often defined by apertures that are comparable to or smaller than the full size of the x-ray beam itself. For instance, in the U(ultra)SAXS configuration, the apertures are 0.1 mm x 0.1 mm and 5 m apart. In comparison, the x-ray beam size at these apertures is likely to be ~95 μ m x 30 μ m, assuming 0.5 μ rad slope error for the KB focusing mirrors. Positional and directional deviation of the x-ray source therefore may result in fluctuations in beam intensity. It can be shown that, in the horizontal direction (aperture size ~ FWHM beam size), the combined motion of the beam at the beam-defining aperture must be less than 8% of the beam size, or 8 μ m, in order to satisfy the 1% intensity stability requirement; whereas in the vertical direction, the allowed beam drift is more than 20 μ m. These requirements are 17 μ m and 54 μ m, respectively, if 5% beam intensity stability is desired. The requirements are much less stringent when the aperture size is relaxed or if the beam size is improved with better focusing optics. The proposed 10% source position (4 μ m) and direction (2 μ rad, 2.5 m arm, 5 μ m) instability each can satisfy the most stringent requirement of <8 μ m horizontal beam drift.

2. Micro-beam SAXS: position and intensity stability

In this configuration, with a target spot size at the sample of a few μ m, the beam is first focused onto an aperture that defines a secondary source (there could also be two separate secondary sources for horizontal and vertical focusing) for the micro-focusing mirrors. The beam at the sample can therefore have very good position stability but its intensity will be determined by the amount of x-ray beam that passes through this aperture, which in turn depends on the positional stability of the source. The size of this secondary source, dictated by the combined requirements of low beam divergence (~0.8 mrad) needed for the purpose of SAXS measurements and small spot size (1 μ m), is ~19 μ m (horizontal, at 45 m, 2:1 focusing for primary KB) by 6.5 μ m (vertical, at 57.5 m, ~1:1 focusing for primary KB). Note that due to the slope error of the primary focusing mirror, the image of the source (25 μ m (H) and 28 μ m (V)) will be much larger than the size of the aperture that defines the secondary source. The proposed 10% maximal source position drift therefore will result in ~1.7% (horizontal, 2 μ m) and ~0.05% (0.4 μ m) change in flux that pass through the secondary source-defining apertures, which is close to the desired 1% beam intensity stability at the sample.

3.7 Stability Requirements for Soft X-Ray Beamlines

The monochromator designs for the initial soft x-ray beamlines at NSLS-II are envisaged to be some sort of variable line spacing, collimated plane grating monochromator (VLS-CPGM). Design variations for ultra-high resolution mode (3600 l/mm) and high flux mode (300 l/mm) were evaluated for the CDR. For those gratings, the expected energy resolution of the beamlines is:

3600 l/mm: 11 meV @ $h\nu = 1000$ eV, 2 meV @ $h\nu = 200$ eV
300 l/mm: 114 meV @ $h\nu = 1000$ eV, 21 meV @ $h\nu = 200$ eV

The main effect of motion in the vertical direction is to produce a degradation of the energy resolution. However, the energy shift of even a very large beam motion of 4 μm in the vertical direction is almost negligible:

3600 l/mm: 0.89 meV @ $h\nu = 1000$ eV, 0.08 meV @ $h\nu = 200$ eV
300 l/mm: 11 meV @ $h\nu = 1000$ eV, 1.0 meV @ $h\nu = 200$ eV

For motion in the horizontal direction, the main impact will be to shift the image at the focus of the last pair of refocus mirrors. However, the demagnification in the horizontal direction is over 50:1. Therefore, even a 10% shift in the source point will produce only a 0.2% shift in the position of the focussed beam.

With regard to stability of the angle of the photon beam, again a 10% criterion will more than satisfy experimental concerns. At that level, the fractional change in the wavevector of the photon beam is about 1 part in 10^{12} in the horizontal direction and 1 part in 10^{14} in the vertical direction.

3.8 Stability Requirements for High Energy X-Ray Beamlines

Superconducting wigglers which produce high energy x-rays can be used as photon sources for angular dispersive x-ray diffraction (ADX), energy-dispersive x-ray diffraction (EDXD), x-ray imaging and radiation therapy research.

For ADXD of large (approximately 1 mm) samples, x-rays are typically focused by a sagittal focusing monochromator at a magnification of approximately unity. A position stability of 10% of sample size results in a source-position stability of approximately 100 μm horizontally and vertically. For ADXD of small samples of a few μm in diamond anvil cells, K-B mirrors (at a magnification of approximately 100:1) are typically used to focus the x-rays. A position stability of 1 μm at the sample requires a source position stability of 100 μm horizontally and vertically. In both cases, wavelength stability of 10^{-4} and usage of a silicon monochromator at a Bragg angle of approximately 0.1 rad require the vertical angular stability to be within 10 μrad .

EDXD experiments that require the most orbit stability are those that use the peak position as a figure-of-merit. These include strain mapping and deformation experiments. For such experiments, the angle of the incident beam is defined by a fixed slit and the source, with the diffraction angle (2θ) typically being 0.1 rad. To obtain 10 micro-strains ($10^{-5} \Delta d/d$) accuracy, the incident angle as defined by the slit and source should be maintained to within 10^{-6} μrad . The source and beam-defining slit being 50 meters apart, the vertical source position should have a stability of 50×10^{-6} meters, or 50 μm .

For imaging (DEI and micro-CT) and micro-beam radiation therapy (MRT) experiments, the distance between the subject and detector is typically 1 meter, and a resolution of ~ 1 μm is typically desirable. Assuming a 50 meters source-to-subject distance, the source position should be stable to within 50 μm horizontally and vertically.

To summarize, for typical superconducting wiggler applications, the source position should be stable within 50 μm horizontally and vertically, and the source vertical angle should be stable within about 10 μrad . There is no requirement on source horizontal angle due to the large horizontal divergence afforded by a superconducting wiggler.

3.9 Stability Requirements for Timing Experiments

NSLS II is expected to serve a number of time-resolved measurement techniques having resolution of ~ 1 ps. This defines a requirement for the phase stability of electron bunches.

Some time-resolved techniques are based on synchronized, ultra-fast lasers. The frequency response of their synchronization systems is highest at low frequencies, becoming less effective above ~ 250 Hz (response of PZT transducers). So electron bunch phase stability is less critical at low frequencies.

3.10 Stability Requirements for XAS Beamlines

Fluctuations in intensity, unless extreme, are handled by normalization. As integration times are generally one to several seconds per data point, x-ray absorption spectroscopy (XAS) is less sensitive to high-frequency instability. Beam position at the sample is a function of source position and angle, and of beamline optics as energy is scanned over a typical 1000 eV. While classic EXAFS samples are perfectly uniform over several mm and thus insensitive to beam position, cutting-edge XAS often involves highly inhomogeneous materials. These require beam position stability of 5-10 μm at the sample (the finest scale of heterogeneity likely to be significant for bulk measurements) over several energy scans. Energy stability is a function of source angular stability and the thermal and mechanical stability of the monochromator. For high-resolution applications, such as phosphorus, chromium, manganese and arsenic K edges and several important L and M edges, spectral features used to differentiate chemical species may differ by as little as 0.1-0.3 eV. Energy stability should then be within 0.05 to 0.1 eV for the duration of an experiment. Source position is generally less of a consideration for bulk XAS, as stability is expected to be within $\sim 10\%$ of source size. Angle of the source beam is more critical, as it influences monochromator energy selection and beam position projected through optics to the sample. For energy stability of 0.05-0.1 eV, a source vertical angle stability of ~ 1 μrad is needed. For position stability, angular deviation can be ameliorated through use of apertures close to the sample, provided the apertures are over-filled by at least the projected position deviation, and this is small relative to the beam size. In contrast, horizontal stability requirements are less rigorous, as the source size and divergence are greater and by nature less of the horizontal extent of generated beam is used. Considerations of stability are compounded by the potential variety of beamline optical components (which can amplify or create instability) and source types (soft bend, hard-bend equivalent, damping wiggler). For vibrational stability, it is expected that final apertures and intensity measurement will be mounted monolithically with the sample stage and detectors. Upstream optics (monochromator, apertures, focusing elements) should be similarly grouped. An active vertical feedback system (as successfully implemented at NSLS X15B) may be necessary to achieve the required stability. While current instrumentation and technology exists for high-resolution monochromator and feedback systems, it is expected that some R&D will be required to combine these aspects for XAS applications at NSLS-II.

3.11 Stability Requirements for XMCD Beamlines using Fast Switching Circularly Polarized Soft X-Rays

For x-ray magnetic circular dichroism (XMCD), the polarization profile of the photon beam is of importance. Changes in the position of the electron beam may or may not influence the polarization ratio between the left and right circularly polarized soft x-rays.

A more extensive study needs to be done to quantify the variations in the polarization ratio, if any, and the impact that this will have in experiments. As an estimate to what is currently possible in sensitivity, currently at X13A we are able to measure the difference signal (in form of hysteresis loops) smaller than 2×10^{-5} . This signal corresponds to the nitrogen hysteresis loops recorded on iron nitrates where the nitrogen is hybridized with the iron.

We will study the case of a beamline with 2 x 2 meters EPU's for NSLS-II for fast switching circularly polarized soft x-rays. Movements in the electron beam in angle across the straight section will not affect too much the polarization ratio if the undulators are completely symmetric respect to the center of the straight section. The polarization ratio will present problems combining shifts and angle movements. In that case the angle will not be centered and different sections of the polarization profile for each insertion device will be extracted. The effect will depend on the polarization profile of each photon beam (how much the polarization changes from the central cone to the extremes of the distribution) and the shift either in horizontal or vertical.

Impact of:	on:	Polarization Ratio	Beam Overlap	Photon Energy
Horizontal shift		no	no	no
Vertical shift		no	no	no
Horizontal angle		no	yes?	no
Vertical angle		no	yes?	yes
Shift and angle		yes	yes?	Yes

3.12 Stability Requirements for Scanning Transmission X-Ray Microscopy Beamlines

- (1) Must have very stable flux on timescales of 0.01-100,000 Hz.
- (2) On that timescale, must have stability in flux to $1:10^4$ or better for transmission experiments.

The flux stability requirement from item (2) above is 0.01%. To provide an estimate of what this requirement means for the NSLS-II electron beam position and angular stability, one can begin with the corresponding analysis for the NSLS STXM beamline X1A from June 2005, and scale appropriately for NSLS-II.

This scaling can be performed using ray-traces based on X1A, which provide intensity sensitivity for position and angle variations of the source in the horizontal and vertical planes. In the horizontal plane, the intensity at NSLS X1A varies by 50% for 500 μm displacement and by 26% for 35 μrad angular rotation. In the vertical plane, the intensity at NSLS X1A varies by 72% for 200 μm displacement and by 56% for 35 μrad angular rotation. Scaling these sensitivities to a requirement of 0.01% intensity stability, the requirements on beam size and angular stability for NSLS-II are: 100 nm displacement and 15 nrad in the horizontal, 30 nm and 6.0 nrad in the vertical.

Note that the scaled values derived above need to be followed up by ray-tracing calculations specific to NSLS-II, since the specific values of source and image size and angular divergence affect the details of the sensitivity results.

The beam stability requirements stated above assume that no mitigating measures will be undertaken at the beamline level, the most obvious of these being faithful monitoring of I_0 in order to normalize the STXM images to (small) changes in the incident beam intensity. Development of such remediating measures is a high priority for STXM beamlines at NSLS-II.

4. Conventional Construction

The role of conventional facilities in assuring beam stability goals for NSLS-II is driven by two primary objectives: (1) providing a structural platform that meets vibration criteria and (2) providing an environment that meets temperature stability criteria. Of these two objectives, the most challenging is assuring that the storage ring tunnel floor and the experimental floor are sufficiently stable to ultimately achieve focused x-ray beam resolution of 1 nm or better.

The source of vibrations affecting NSLS-II are pre-existing or cultural vibrations related to the selected site, vibrations due to the machine itself and vibrations generated by the supporting facilities. Cultural vibrations are a function of the geologic conditions transmitting vibration to the site and proximity to surrounding sources such as road traffic and machinery in adjacent facilities. Vibration sources due to the machine include the flow of cooling water through devices, the physical support systems and electromagnetic forces. Vibration sources associated with supporting facilities include power, cooling, HVAC and foot traffic associated with operation of the light source buildings and ancillary systems. Facility vibration sources and to a lesser extent, cultural vibration sources, are heavily influenced by the layout, structural and mechanical design of the light source facility and its support systems within the scope of conventional facilities.

Ground motion at the NSLS-II site has a complex spectrum consisting of fast and slow motion. Slow motion characterized by long wavelengths is the result of ocean swells, wave action and crustal resonances (a few Hz depending on the structure of the subsurface). Waves arriving at the site with wavelengths larger than the diameter of the NSLS-II will not affect the stability of the beam. Cultural noise on the other hand with frequencies higher than a few Hz has the potential of dramatically affecting its performance through the coupling that exists between lattice movement and beam distortion or jitter, especially when the motion is uncorrelated. In order to achieve the desired stability in the accelerator beam, the uncorrelated band of cultural noise must be kept at a minimum since it is the dominant source of beam jitter.

While the first line of defense is the selection of a quiet site characterized by reduced levels of vibration throughout the uncorrelated frequency band and especially the band segment within which the fundamental frequencies of systems supporting the lattice magnetic elements are found, that alone does not suffice. Cultural noise within the critical frequency band generated by accelerator-related systems will inevitably be generated and travel around the facility. Therefore the role of the structure (its design as well as its interface with the supporting medium) is critical.

At rock sites, with an accelerator foundation of any thickness, the floor will assume the vibration levels of the free-field. In the case of a soft site, the placement of the foundation will alter the free-field motions by filtering out a wavelength band associated with the dimensions of the structure. Rock sites, on the other hand, are more susceptible to cultural noise generated by operating equipment in the vicinity of the structure than soft ground counterparts. Therefore, determining in advance, the specific interaction between the foundation structure and the free-field environment as well as the anticipated induced vibrations is essential for design of sensitive facilities. The stability of the operation at levels demanded by the next generation light sources like the NSLS-II can only be met

through a fully coupled, complimentary relationship between the performance goals driving the accelerator stability requirements, the NSLS-II site ground motion environment and the design of the structural elements of the accelerator.

Discussed below are: (a) the NSLS-II site and its established ground vibration environment under green-field conditions including comparison with vibration stability experience from operating 3rd generation light sources; (b) quantification of ground motion criteria for the accelerator ring and the experimental floor; (c) an overview of the on-going studies aiming to arrive at design features that will help keep the uncorrelated motion at a minimum thus ensuring stability of the beam; and (d) a list of R&D activities to be pursued that will help in understanding the relationships between ground motion and beam jitter as well as exploration of noise suppression techniques or structural design features.

4.1 NSLS-II Site and Ground Motion Environment

Geophysical studies conducted at the BNL site over a number of years suggest that the NSLS-II will be built on generally uniform, well-settled glacial sands forming a well-characterized 1400-foot layer above the bedrock. The water table, which is an important feature to be considered in establishing the ground motion environment including its frequency content, is situated at approximately 30 feet below grade (~ 10m). The shear wave velocity in the upper strata of the subsurface has been estimated to be 886 ft/sec. Given that the coherence in ground vibration, which in turn is affected by the variability in geologic conditions at any given site, is a very important parameter in ensuring that the spatial variation of motion in a sensitive facility is kept at a minimum, the homogeneity exhibited by the NSLS-II subsurface will help minimize spatial variability in ring floor motion.

In general, a rock site is preferable for a sensitive facility such as the NSLS-II due to the significant reduction of cultural ground motion that occurs as a result of the absence of surface layer made of much softer material which can trap or amplify waves propagating through it. On the other hand, homogeneous, well-settled sandy subsurface exhibits properties that are superior to those of a rock site in terms of filtering ground motion arriving at the site as a result of foundation/soil interaction and arrest of facility-generated noise from operating systems. The impedance difference between the accelerator foundation and the subsurface it is laying on, which is higher in the case of a sandy subsurface, plays a key role in reducing ground vibration on the ring or the experimental floor due to vibration from rotating machines on a near-by but separate foundation. In the case of a hard rock site, however, the impedance difference between the supporting ground and the facility floor is minimized, allowing the rock to act as a conduit of noise generated in the nearby facilities.

To assess the ground vibration that exists at the NSLS-II site under “green-field” conditions, field studies have been performed and results were compared with free-field conditions that exist in other facilities. Figure 4.1 depicts power spectral densities of representative vertical daytime and nighttime motions measured at the NSLS-II site. The NSLS-II green-field spectra are compared in Figure 4.2 with measurements at two key locations of the Spring-8 facility which represents the quietest of all the light source sites. Also listed in Figure 4.2 is the integrated rms vertical displacement for the frequency range of 2-100 Hz. The two measurements at the Spring-8 free-field at a location of rock outcrop outside the ring perimeter exhibit vertical displacements of 2-3nm while the third

measurement made on the surface of a soil layer~ overlaying the Spring-8 rock and near the long experimental line end-station exhibits vertical rms displacements higher than those measured at the NSLS-II site (~20 nm). While the measurements at the NSLS-II site represent free-field conditions, it is expected that upon placement of the facility foundation structures, and due to kinematic interaction that results in wave scattering, the “green-field” ground motion will be filtered by the structure leading to lower integrated displacements on the ring floor. In order to validate the filtering effect, measurements were performed using the CFN facility foundation, which rests on similar soil as the NSLS-II, as the test bed. Figure 4.3 reflects the positive role played by the CFN foundation mat in reducing the vibration levels that exists in the near-field. To assess the level of reduction that may be realized when the NSLS-II facility is placed on the selected site, large-scale models that describe both the facility and the subsurface were used for the propagation and scattering of the waves that constitute the green-field motion. Figure 4.4 represents an early estimation of the reduction anticipated.

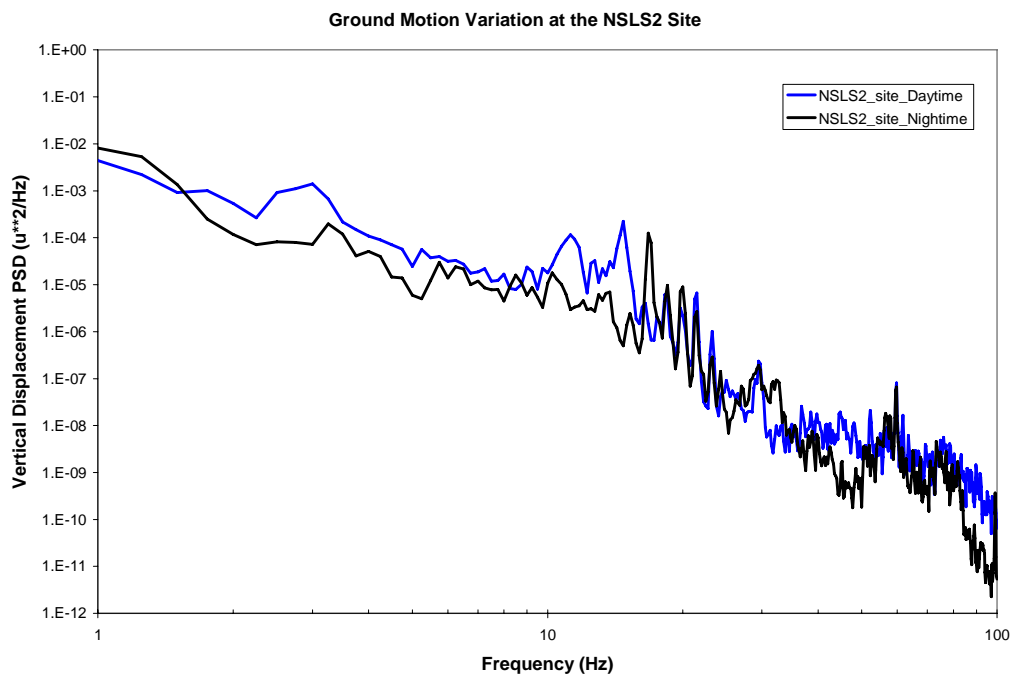


Figure 4.1: Vertical displacement PSD measured at the NSLS-II “green-field” site showing variations between daytime and nighttime

Free-Field Ground Vibration Levels at SPring-8 and NSLS II Sites

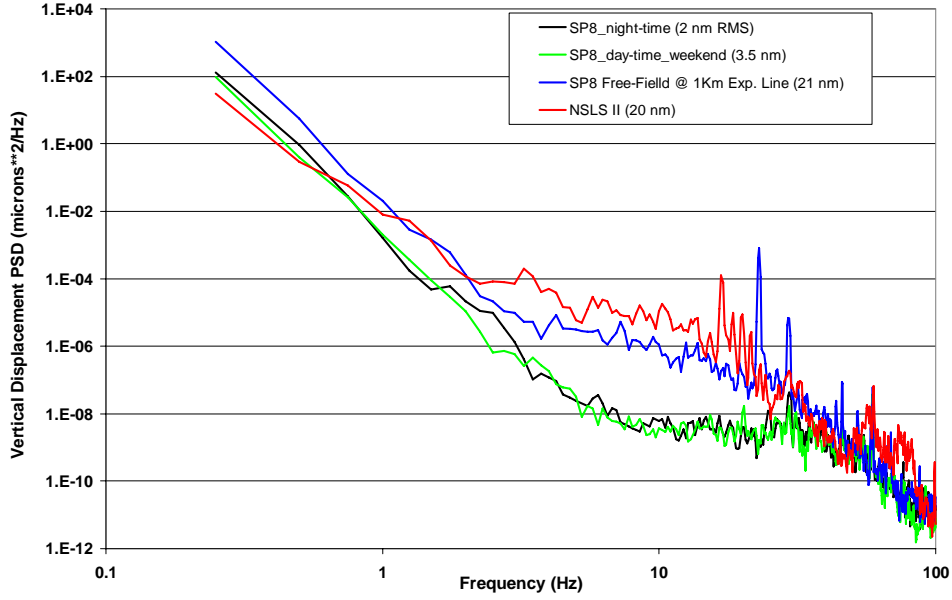


Figure 4.2: Vertical displacement PSD measured at the NSLS-II and Spring-8 sites

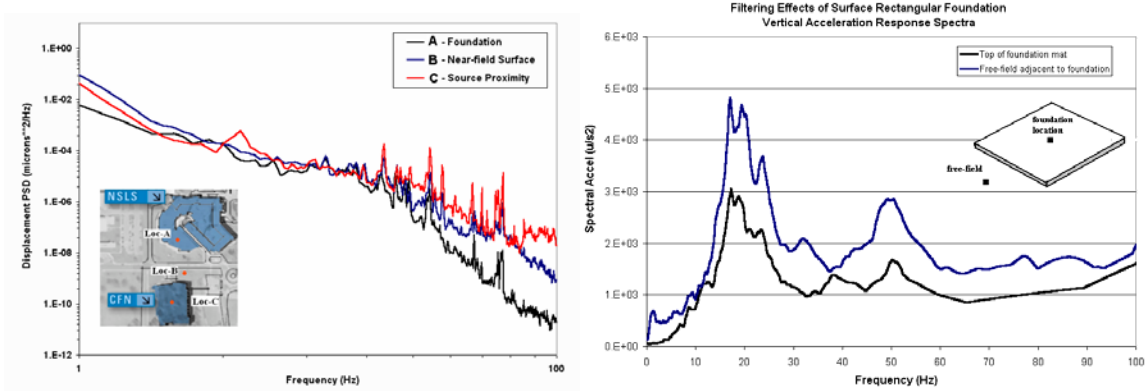


Figure 4.3: Filtering of the free-field ground motion measured at the CFN floor. Fig. 4.3a shows the attenuation path of the cultural noise generated at the NSLS facility. Fig 4.3b depicts the resulting reduction in the response spectra between the CFN near-field and the CFN floor.

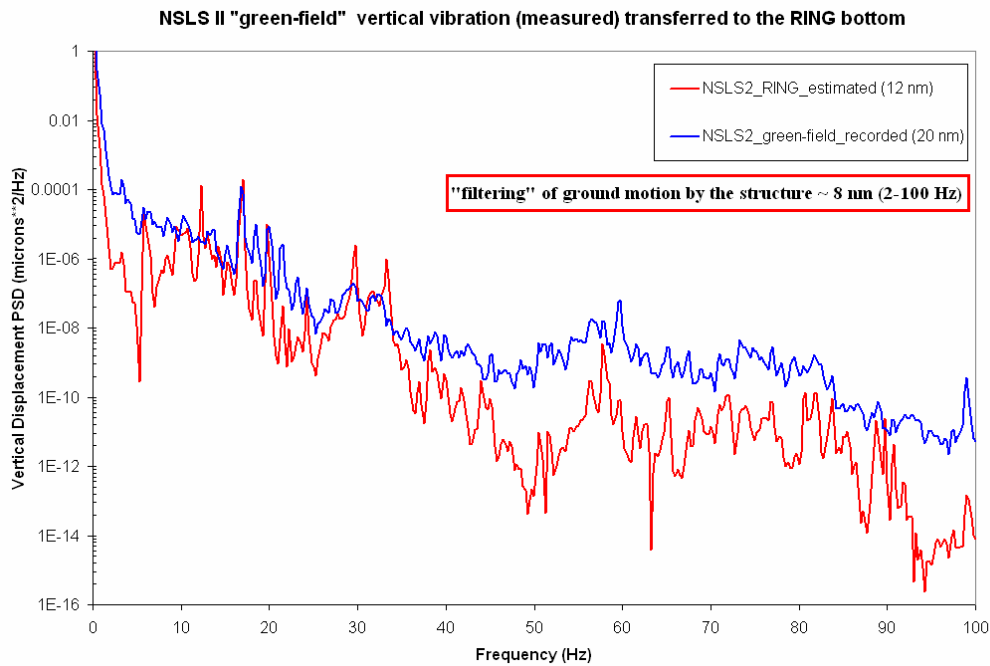


Figure 4.4: Expected filtering of the free-field ground motion measured at the NSLS-II “green-field” floor due to the placement of the NSLS-II ring and experimental floor

4.2 NSLS-II Storage Ring and Experimental Beamline Stability Requirements

The requirements for the NSLS-II storage ring floor stability stem from the uncorrelated part of the ground motion that is expected to reach the floor and propagate around the ring inducing distortions in the relative position of the magnetic elements in the lattice. As mentioned above, ground motion waves reaching the ring floor that are of the order of the betatron wavelength or smaller (**~13 m**) are the ones that are of concern because of the lack of correlation that they exhibit.

Slow ground motions with wavelengths larger than the characteristic dimensions of the accelerator (i.e. diameter) or with characteristic frequencies below 1 Hz do not have serious effects on the stability of the beam despite the fact that they result in much larger floor displacements because the motion they induce is correlated and can be appropriately corrected. For example, ocean wave action with characteristic frequency of about 0.2 Hz and a surface wave wavelength of ~1,200 m (~4,000 feet) is expected to have space and time coherence. Correlation studies have also shown that the “slow” band of the fast motion or cultural noise (band between 1 and 6 Hz) is highly correlated and therefore can be easily corrected. Thus, it is the incoherent nature of the fast motion (mostly cultural noise) reaching the ring floor and exhibiting characteristic frequencies higher than a few Hz (> 6 Hz) that will induce distortions in the beam. As a result, the integrated displacement for the range of interest (range that encompasses the fundamental frequencies of lattice magnet systems supported on the ring floor and expected to amplify the floor motion) must be kept as low as possible. Based on relations that link ground motion with beam jitter (i.e. establishment of response functions between the movement of a lattice magnetic element and jitter on the beam) while taking into account anticipated vertical motion amplification between the ring floor and the magnetic element reference, the upper limit of the tolerated

rms vertical displacement at the ring floor level and for the range between 4-50 Hz has been set at **25nm**.

The sources are the external (natural/cultural) and the self-generated. To ensure that the vibration criteria for stability are met, design features must be implemented that maximize attenuation of cultural as well as self-generated vibration sources. These design features include optimization of floor thickness, monolithic tunnel structure with the experimental floor, isolation from the operating mechanical systems and selection of well-balanced machinery.

The ground vibration measurements at the NSLS-II site (~20 nm in 2-10 Hz) aided also by the expected filtering (shown in the case of CFN) due to the interaction of the NSLS-II floor structure with the supporting soil, indicate that the requirement of maintaining the uncorrelated vertical displacement (< 25nm for the 4-50 Hz range) is achievable. Recent vibration studies conducted on the experimental floor and the storage ring foundation of the APS which is subject to similar geologic and cultural noise conditions indicate that the two important criteria namely the 25 nm rms vertical ring floor displacement and the minimization of the differential movement between locations on the experimental floor to an order of 1 nm or less can be realized, with the latter requiring special design of the experimental floor section supporting extremely sensitive beam lines.

While the overall requirements for stability of the experimental lines having their infrastructure supported on the experimental floor mat are inevitably coupled and driven-by requirements established for the ring, there are special requirements needed to be met on the experimental floor in order to satisfy the variety of sensitivities that characterize experiments at the end stations. This stems, primarily, from the 1nm X-ray optics desired by some of the experimental lines. From the structural point of view, the desired criteria for both the ring and the experimental lines can be met with careful consideration of (a) the ground vibration environment at the NSLS-II site, (b) implementation of special structural features that maximize the filtering of ground motion and minimize the differential movement between the ring and the experimental floor, and (c) designing the experimental station support infrastructure in close relation to the floor motion amplification characteristics and thus minimizing differential movements between the reference beam position and the imaging point.

The stability requirements on the NSLS-II experimental floor can be separated into two groups, specifically, the 1nm-level sensitivity lines and experimental lines such as infrared that desire beam motion limits below 0.25 μ m. The stability of either group is inherently linked to the electron beam stability whose jitter is a function of the movement of the ring floor. Taking into consideration that ground motion can be divided into “fast” and “slow” regimes (fast being the motion above a few Hz and assuming increased time and space incoherence with increased frequency) a desired upper limit of vertical ring floor displacement (rms) has been set at 25nm for the fast motion covering the range between 4 and 50 Hz. It should be pointed out that due to structural differences between the NSLS-II ring and the experimental floor (ring foundation mat has higher thickness that provides both global rigidity and vibration filtering), the rms vertical displacement on the experimental floor is expected to be slightly higher than its ring counterpart. The temporal and spatial variability that is expected to be seen on the experimental floor (also observed in other operating light sources) will require special care in order to satisfy the requirements of very sensitive experimental lines. Figure 4.5 depicts spatial and temporal

variation in measured power spectra density (μ^2/Hz) and the rms vertical displacement at two locations on the Spring-8 experimental floor separated by 90m distance.

To ensure that the vertical differential motions between two locations on the experimental floor supporting the most sensitive experimental lines requiring imaging resolution of the order of 1nm is minimized and can satisfy the stringent requirements, structural enhancements need to be implemented. Specifically, by supporting the last optical element of the 1nm resolution line and the imaging point on the same support structure which is designed with dynamic properties that fall outside the motion amplification regime of the floor motion will ensure that the differential movement of these two key reference points is eliminated. Further, by creating a rigid link between the extraction point and the imaging point (achieved by enhancing the floor mat thickness locally which will provide the rigidity required) the differential motion of distant locations on the experimental floor can be minimized. The motion isolation of experimental floor sections supporting sensitive lines can further be enhanced with special structural features that will help interrupt the propagation of waves traveling on the experimental floor. The synergy between the structural enhancements, the understanding of the floor motion frequency content and amplification characteristics and the active feed-back and correction will ensure that stability which can support the 1nm resolution imaging can be achieved.

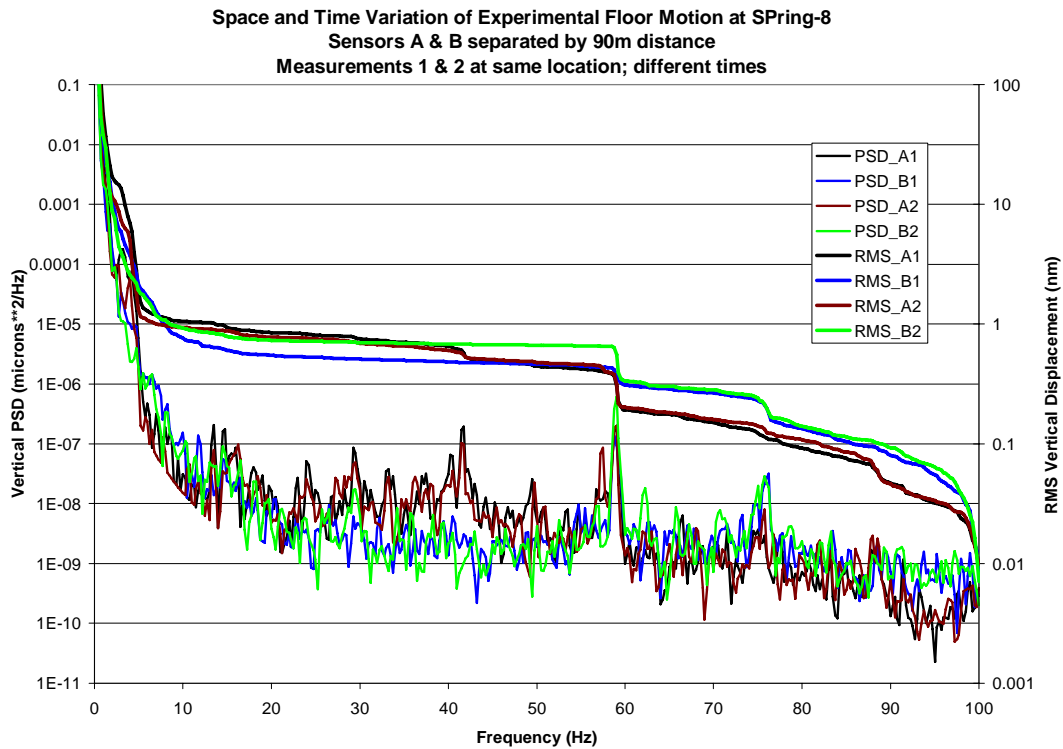


Figure 4.5: Measured displacement power spectral densities and rms displacements on the Spring-8 experimental floor demonstrating both temporal and spatial variability of floor vertical motion

4.3 Structural Considerations

In an effort to predict the vibration characteristics at the ring and experimental floors subject to the existing natural noise environment and the anticipated cultural noise from the NSLS-II operating systems, an extensive analysis based on detailed modeling of the site and the structures that are expected to play a role in both the generation of vibration as well as its filtering has been initiated. The primary goals of this comprehensive analysis/simulation of ground motion interacting with the NSLS-II facilities are: (a) the optimization of the ring floor thickness while meeting the set criteria for vertical rms motion; (b) estimation of the contribution of NSLS-II system-generated noise towards the threshold criteria and the identification of the optimal configuration that interferes in the propagation of self-generated noise including structure-to-structure interaction; (c) assessment of special noise path interruption features that will help minimize cultural noise traveling on the experimental floor towards extremely sensitive lines.

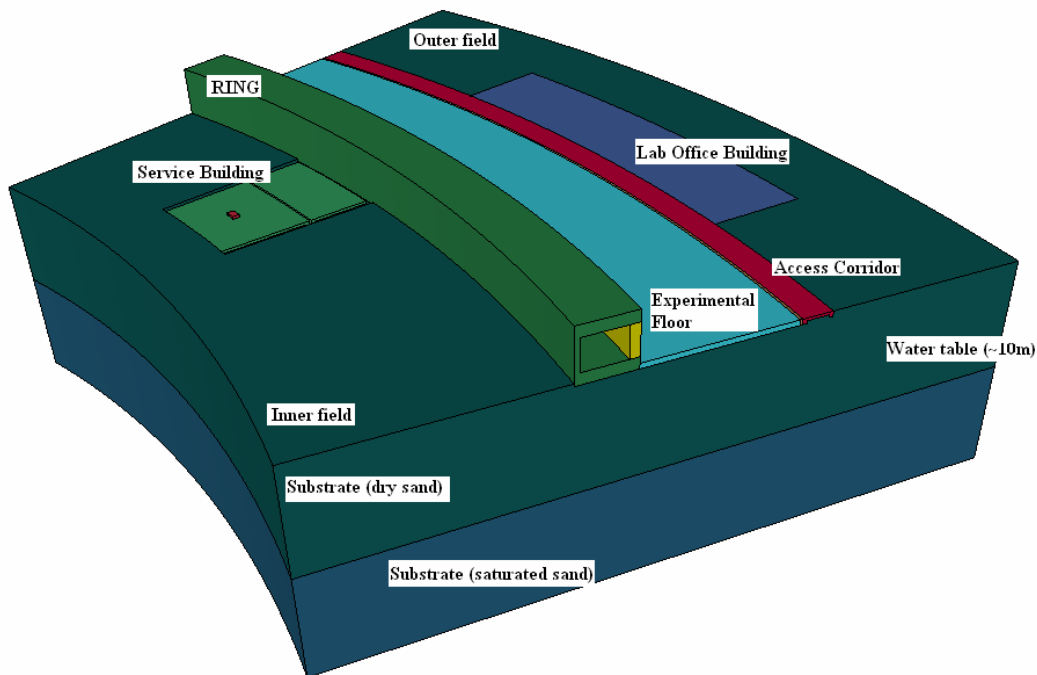


Figure 4.6: Structural details of the interfaces between the NSLS-II ring, the experimental floor and the service buildings (baseline option)

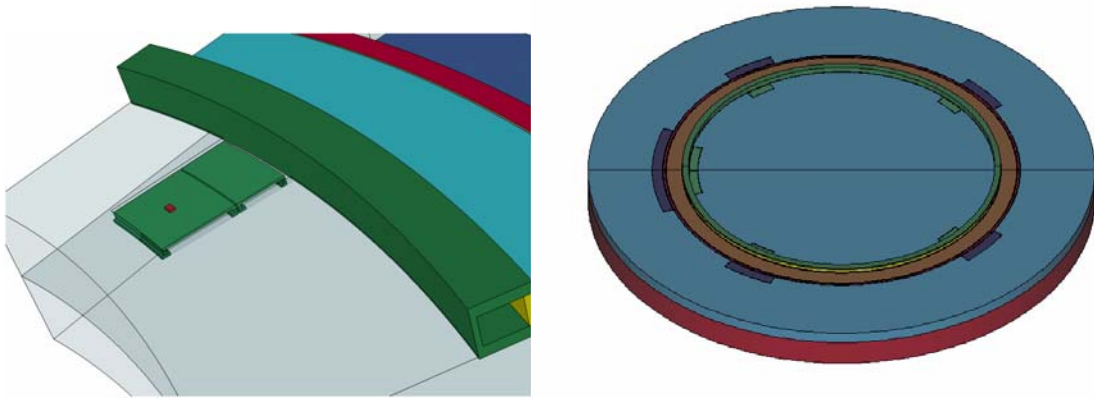


Figure 4.7: Interface and structural details of the service building floors. Shown is the partitioning of the mechanical room and the option to house the operating systems on the outer section in order to minimize facility-generated noise on the ring floor. Figure 4.7b is a depiction of the complete model generated to study the interaction of the NSLS-II facility with the ground vibration (natural and cultural) at the proposed site

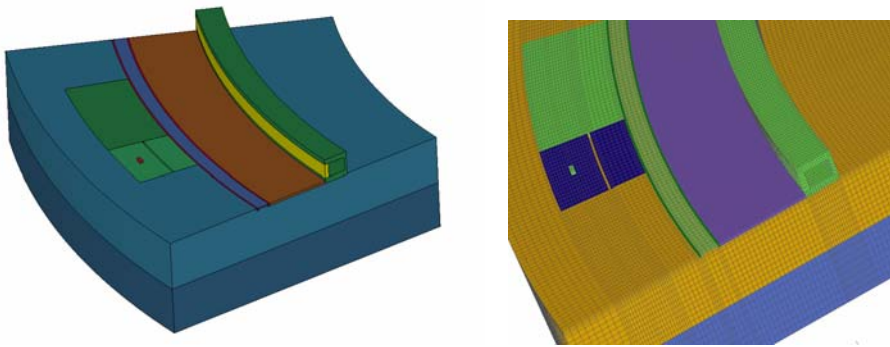


Figure 4.8: Alternative layout option affecting the location of the NSLS-II service buildings being explored to enable further minimization of in-house generated cultural noise from facility operations

Figures 4.6, 4.7 and 4.8 are finite element representations of the closely coupled structural elements of the NSLS-II accelerator including the supporting surface soil layer and the layer below the water table. Studies to-date focused on the scattering and attenuation characteristics of noise generated on the service building foundation, the access corridor and the free-field. In anticipation that the bulk of the self-induced noise will originate on the service building floor, attenuation options that include, but are not restricted to, the increase of distance between the ring floor and these sources are being explored (see Figure 4.6). To help guide the optimization effort, vibration measurements in the proximity of operating mechanical equipment such as chillers and pumps were conducted at other facilities. Results shown in Fig. 4.9 indicate the significant attenuation that occurs even at small distances ($\sim 2\text{m}$) away from the supporting pads. In addition, the effectiveness of special isolation joints was studied at the two facilities (APS and Spring-8) for implementation into the design of the NSLS-II service building and experimental floor.

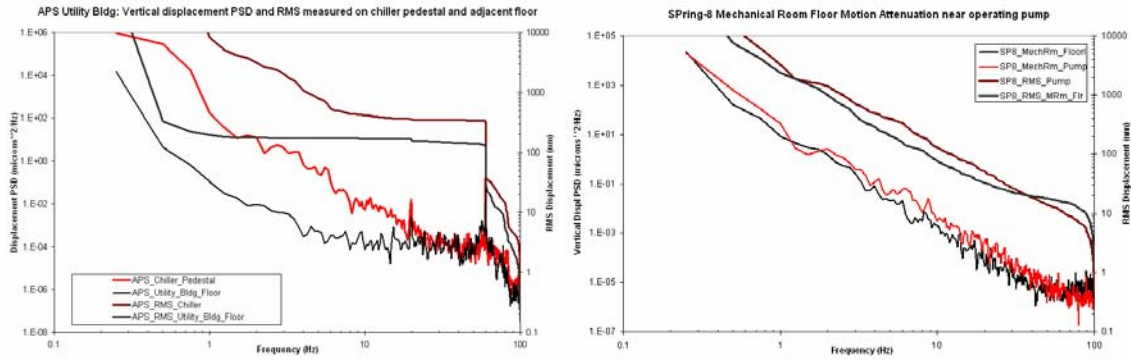


Figure 4.9: Motion attenuation studies on the floors of utility buildings serving the APS and Spring-8 facilities

Based on past experience, actual field measurements at different facilities (including NSLS, APS, Spring-8, CFN, etc.) and the to-date results of the detailed analyses, the following structural considerations have been used in guiding the design of a “quiet” facility that will meet the required stability criteria:

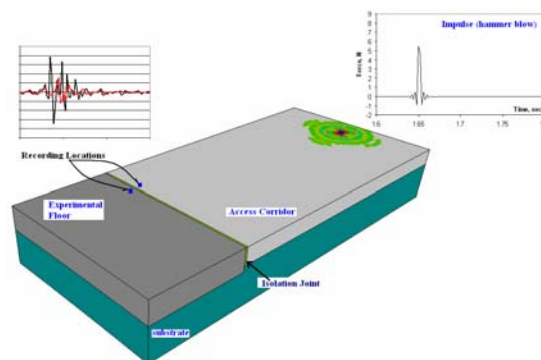
- Maintaining a monolithic structure between the ring and the experimental floor to maximize filtering of ground motion present at the site
- Maintaining a structural “box beam” structure for the accelerator tunnel to stiffen the tunnel floor and adjacent experimental floor
- Enhancement of the experimental floor thickness supporting the most sensitive experimental lines to form a “rigid” connection between the beam extraction (reference point) and the focal point at the end of the line leading to the minimization of differential movement
- Minimization of the amplification of motion between the experimental floor and the elevations of interest (reference and focal points) by selecting the dynamic properties of the support structures according to the frequency content of the floor motion (including base isolation) and by mounting the last focal element and the focal point on the same support
- Consideration of arresting noise generated on the experimental floor and propagating towards the sensitive experimental lines by introducing special isolation joints (trenches) that disrupt the propagation of motion on the floor acting as a wave guide but do not reduce the overall ring/experimental floor rigidity.
- Implementation of special isolation features between the experimental floor and the outer accelerator structures that are subject to noise generation. Recent field measurements at the APS floor demonstrated the effectiveness of such isolation features

4.4 Validation Efforts

In an effort to ensure that both the interaction of the NSLS-II facility with the natural noise environment and the propagation/mitigation of the cultural, in-house noise are properly assessed, given the stringent stability requirements, a comprehensive analytical effort has been launched to both allow for: (a) the best possible estimates of noise levels on the NSLS- II ring and experimental floors and (b) evaluation of different layout options of the facility and the interfaces between key structures. The analytical effort is based on wave propagation and scattering through an explicit finite element analysis that enables the

modeling and consideration of all important structural and interface features. While the adopted analytical/numerical approach has been extremely successful in the recent past in predicting the dynamic response of complex structures, a series of validation efforts which are more relevant to the NSLS-II project have been undertaken to ensure that the methodology can predict ground and facility vibrations at the micro- and nano-levels. These field experiments, which were followed by verification analyses based on the finite element-based simulation model, include:

1. Hammer (impulse) test on the APS floor to assess the effectiveness of isolation joints and enable the validation of the finite element model in predicting the amplitude and the structure of the transients on the floor and across these special joints. Figures 4.10a and 4.10b depict the test setting and the representative result comparison respectively.
2. Cultural (in-house generated) wave propagation and motion attenuation at the BNL RHIC accelerator facility that is subject to similar ground conditions to those of the NSLS-II site. In particular, the attenuation of frequency-rich ground motion records induced by the operation of large compressors was studied using the “unspoiled” conditions surrounding the operation of a large compressor unit in one of the mechanical facilities of the RHIC accelerator during a maintenance day when all other primary sources in the proximity were turned off. Figures 12a and 12b show the actual experimental setting and the comparison between the measured and the predicted vertical displacement power spectra density functions.
3. Cultural wave propagation and attenuation as well as filtering effects associated with ground motions made-up from a multitude of sources and frequencies. In particular, the attenuation characteristics of the complex ground motion generated by the operating systems at the NSLS facility and the filtering characteristics of the CFN facility foundation were both measured and analyzed using the developed analytical model.
4. Benchmarking of the propagation of cultural ground motion generated by a large pump operating in the mechanical room of the Spring-8 facility. The effort is based on actual data measured at the facility and is focusing on the floor vibration attenuation due to a multitude of isolation joints between the mechanical room and the storage ring.



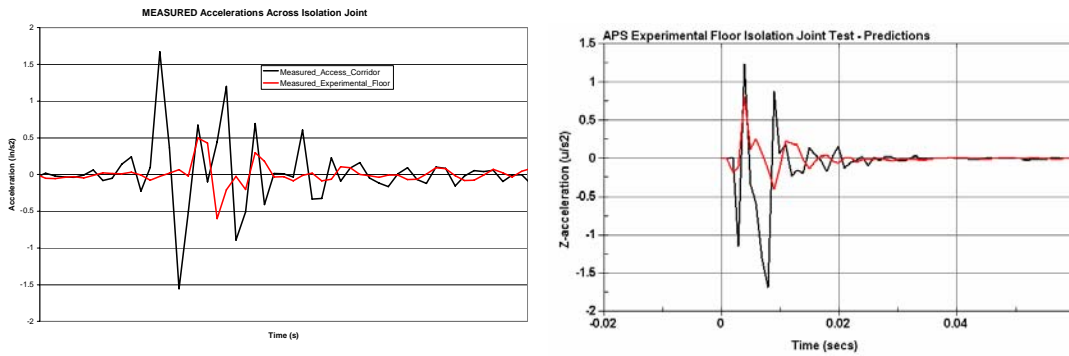


Figure 4.10: APS floor impulse test description and comparison of experimental results with model predictions

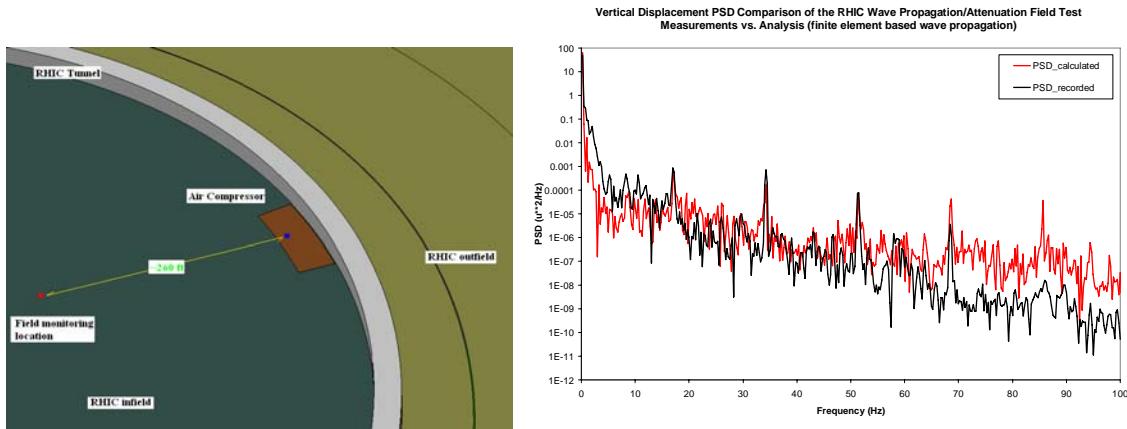


Figure 11: RHIC facility wave propagation and attenuation experiment. Field test layout and power spectra comparison between the experimental and analytical results.

Detailed discussion of the analytical model benchmarking effort will be described elsewhere. The following can be summarized as a result of the experimental data analysis and its comparison with the finite element-based analysis predictions:

- The adopted finite element formulation and the generated finite element models that include all the primary features have been shown to closely predict the experimental data both in terms of amplitude and frequency content.
- Based on (a) the model validation achieved, and (b) the versatility of the comprehensive model(s) that enable the consideration of structural details or layout options and, most importantly, (c) the action of multiple sources simultaneously, sensitivity analyses can be performed to address uncertainties in controlling parameters (i.e. distance, soil and structural damping, interfaces, etc.) as well as to perform optimization studies for storage ring and experimental floor thickness.

4.5 Thermal Stability

Thermal stability of the storage ring tunnel environment, and to a lesser extent the experimental floor, is required to minimize the effects of thermal expansion/contraction of machine components. This is most critical in the storage ring tunnel where temperature changes can cause deflection of the girder system supporting storage ring components. For this reason, the most demanding temperature stability requirement is to achieve stability of $\pm 0.1^{\circ}\text{C}$ in the tunnel. Temperature stability on the experimental floor is not as critical and can be maintained at $\pm 0.5^{\circ}\text{C}$ or nominally 1°F . There will be applications where more stringent temperature requirements will apply within hatches on the experimental floor. These applications will be addressed within the design of the experimental beam lines.

The ability to achieve thermal stability of $\pm 0.1^{\circ}\text{C}$ within the storage ring tunnel has been demonstrated at other Light Source facilities and other facilities at BNL. The relatively stable nature of the load and heat rejected to the space makes this requirement quite achievable when coupled with well designed HVAC systems that utilize high precision/high resolution instruments and controls and air handling equipment capable of being modulated to achieve precise outlet conditions. BNL has installed similar systems in high accuracy laboratory settings that have achieved stability performance of 0.05°C . Additional modeling of airflow and temperature distribution will be performed to assure these techniques are consistent in the tunnel environment.

The ability to achieve thermal stability of $\pm 0.5^{\circ}\text{C}$ or nominally 1°F on the experimental floor is readily achieved by commercial HVAC systems provided proper attention is placed on selection of industrial grade instrumentation, location of instrumentation, control logic, proper distribution of supply and return airflow and limiting variability of external sources such as direct sunlight, infiltration or poorly insulated surfaces.

Conventional facilities will also provide chilled water and tower water for cooling of process water systems used to cool accelerator components. Temperature control schemes for process cooling water are described in the Mechanical Systems section of this report. Additionally, conventional facilities will provide feedback of the status of key conventional facilities systems parameters for monitoring and use in the accelerator control system.

4.6 Envisioned R&D on Vibration Stability of Conventional Facilities

The envisioned R&D will focus on both the floor motion characteristics which are site-specific as well as structure-specific and on the effectiveness of design features that will enable the suppression of floor motion (both absolute and relative). The major efforts will include:

- Continuous monitoring of the NSLS-II site and establishment of temporal as well as spatial variations of the vibration environment including source/path identifications, spectral content and correlation. The effort will include dedicated R&D in studying site-specific slow ground motion (<0.01 Hz) which, even though it has all along been considered to have complete space and time coherence, may be dominated by residual inelastic and non-correlated components that will ultimately have an effect on the beam.
- Field studies at operating light sources while focusing on analyzing systems that are responsible for in-house cultural noise
- A detailed study of the ground motion expected to filter through the ring and the experimental floor including its spatial variability, response spectral characteristics as well as correlation properties. This will combine green-field ground motion measurements and global NSLS-II structure interaction
- Measurement of flow-induced vibration in other operating light source facilities and benchmarking of detailed numerical models capturing vibration amplitudes, frequency content and propagation characteristics. Optimization of the coupling between cooling systems prone to inducing vibrations with the NSLS-II ring and experimental floor
- Assessment and optimization of effectiveness of varied design approaches for structural and mechanical systems in minimizing vibrations reaching the accelerator floor
- Assessment of the effectiveness of experimental floor structural features (i.e. local mat thickness enhancement, trenching, base isolation, etc.) through benchmarked numerical studies that will help guide the design of the sensitive experimental lines.
- Thermal dispersion modeling and analysis to assess and optimize designs to achieve tunnel temperature stability objectives.

5. Mechanical Systems

5.1. Mechanical Stability Requirements

Storage ring girders provide a common mounting platform for the dipoles and multipole magnets including correctors. They also support vacuum chambers on which 7 of the 9 BPM buttons of a cell are flange-mounted. Mechanical stability of the girders, magnets and vacuum chambers are, therefore, critical to providing a stable beam to the users.

Various sources such as ambient floor motion, flow-induced vibration and thermal transients [Ref.5.1] can affect the mechanical stability of the girder assemblies. Based on the beam stability criterion of 10% of the beam size, tolerance limits for random magnet and girder motions in the vertical and horizontal directions were established as shown in Table 5.1.

Table 5.1. Tolerance Limits on Random Motion

Tolerance Limits	ΔX RMS Quads	ΔY RMS Quads
Random magnet motion	$< 0.15 \mu\text{m}$	$< 0.025 \mu\text{m}$
Random girder motion	$< 0.6 \mu\text{m}$	$< 0.07 \mu\text{m}$

Since the beam size in the vertical direction is 10 times smaller than in the horizontal direction, the tolerance requirements in the vertical direction are more stringent. The design and analyses of the magnet-girder-vacuum chamber support system presented in the following sections will focus on the motion in the vertical direction.

5.2. Conceptual Design of the Storage Ring Girder Support System

a) Storage Ring Girders

A conceptual design for a typical girder with its mounting pedestals is shown in Fig. 5.1. The nominal length is approximately 3.0 m for the dipole girders and 3.2 to 6 m for the multipole girders. The girders are approximately 0.8 m wide and 0.4 m high. They will be fabricated by welding commercially available ASTM A-36 steel plates and channels of thickness ranging from 1 to 2 inches. After welding, the girders will be stress-relieved by vibratory stress-relief equipment.

Since the ambient ground motion decreases sharply as inverse of the fourth power of frequency, the girders are designed to achieve natural frequencies of greater than 50 Hz. To achieve this, 7 plates of 1-inch thickness will be welded to the girder to increase its stiffness in torsion. The natural frequency of the NSLS-II magnet-girder support system will be further improved by eliminating elaborate alignment mechanisms. Additionally, lowering the beam height to 1m in the tunnel allows for low-profile stiff girders. The girders will be mounted on 2-inch thick steel pedestals that are grouted to the floor with a non-shrinking epoxy grout. For mounting and height adjustment, eight 2-inch diameter bolts with steel washers will be used.

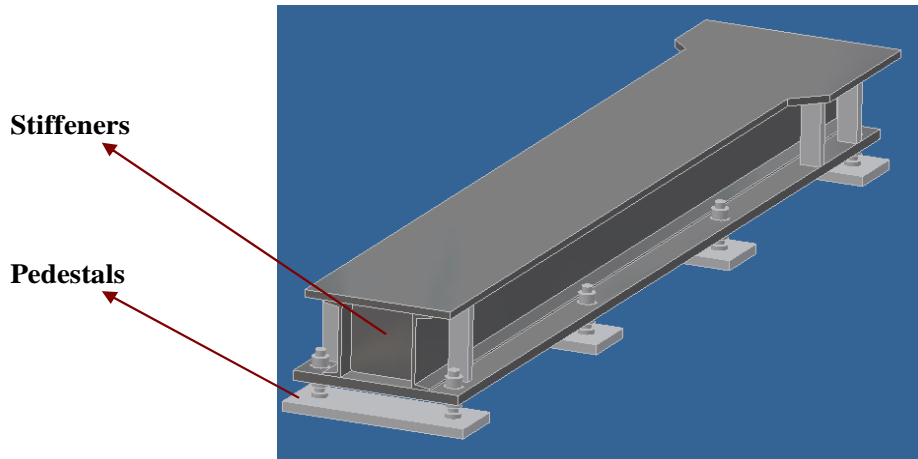


Figure 5.1: Conceptual design of NSLS-II storage ring girder

(b) Vacuum Chamber Supports

Each vacuum chamber will be supported by stands made from Invar 36 which has a low coefficient of thermal expansion, $1.3 \mu\text{m} / \text{m} / ^\circ\text{C}$ (approximately 10 times lower than that of stainless steel). The Invar plates will be approximately 16-inch in height and 0.25 to 0.5-inch in thickness. The BPM buttons will be mounted as close to the chamber supports as practical.

5.3. Mechanical Stability of the Magnet-Girder Support System

a) Thermal Stability

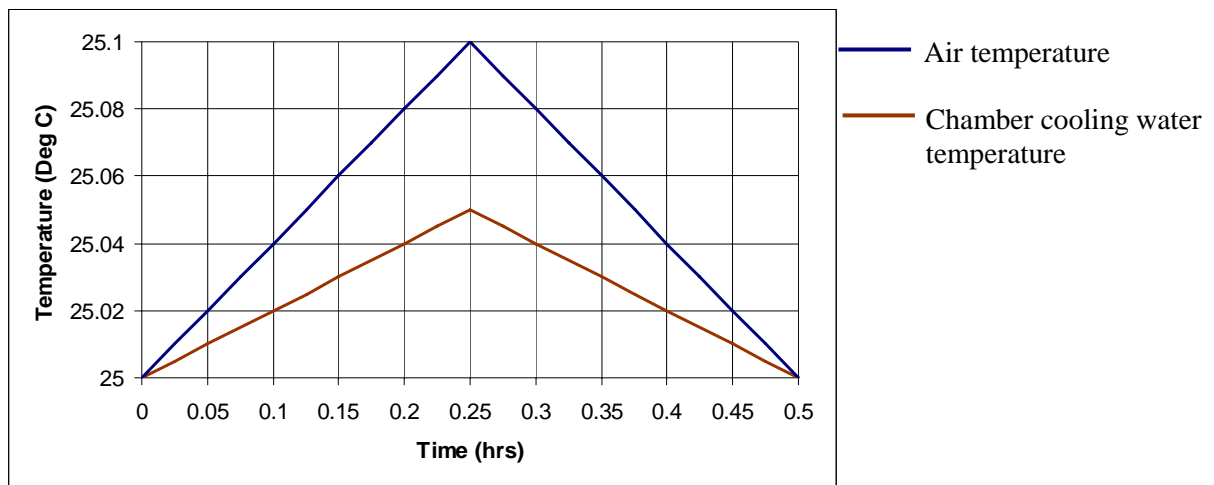


Figure 5.2: Fluctuations in the tunnel air temperature, and process water temperature

Fluctuations of the tunnel air temperature and process water temperature will result in displacements of both the magnets on the girders and the BPMs mounted on the vacuum chambers. To insure, that the thermal deformations of the ring components are acceptable and within the design specifications the following design guidelines are used:

a) The process water and tunnel air temperature fluctuations are specified to be within ± 0.05 °C and ± 0.1 °C respectively. Also one-hour cycles are specified for both the air and process water temperatures to take advantage of the large thermal inertia of the girder system,

b) As reported in the experimental study of thermal deformation of the magnet girder at the SRRC storage ring [Ref.5.2], [Ref.5.3], by insulating the girder the thermal deflection can be minimized by a factor of 2. For the NSLS-II girder, the side channels of the girder will be provided with a 2-inch thick layer of insulation.

To investigate the effect of temperature transients, FE thermal analyses were done for the girder, magnets and vacuum chamber assembly. For the analyses, the fluctuations in the temperature of the tunnel air and the cooling water flowing through vacuum chamber were approximated by linear curves as shown in Fig. 5.2. For modeling heat transfer by air convection, a film coefficient value of $8 \text{ W/m}^2 \text{ }^\circ\text{C}$ and $1 \text{ W/m}^2 \text{ }^\circ\text{C}$ was applied on all external surfaces and internal girder's surface respectively. The lower film coefficient value was applied on the internal girder's surface to include the effect of stagnant air condition.

For modeling heat transfer by process water a film coefficient value of $15,000 \text{ W/m}^2 \text{ }^\circ\text{C}$ was applied. For girder insulation a glass-wool material with a thermal conductivity of $0.03 \text{ W/m }^\circ\text{C}$ was considered in the analysis.

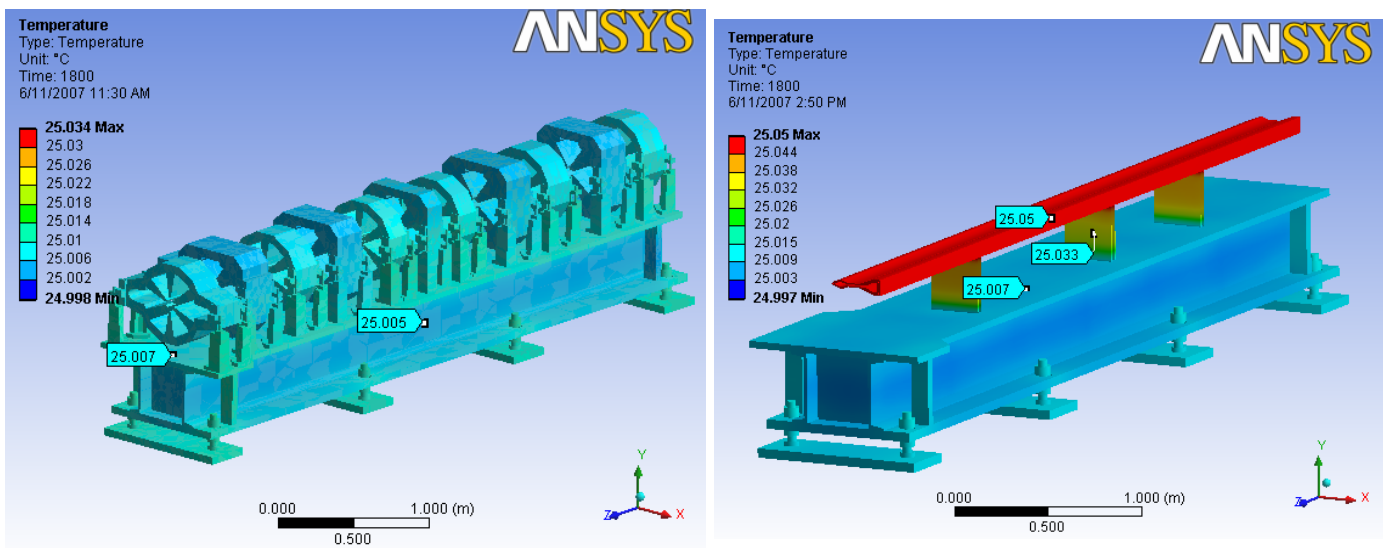


Figure 5.3: Temperature distribution in the girder, magnets and vacuum chamber assembly

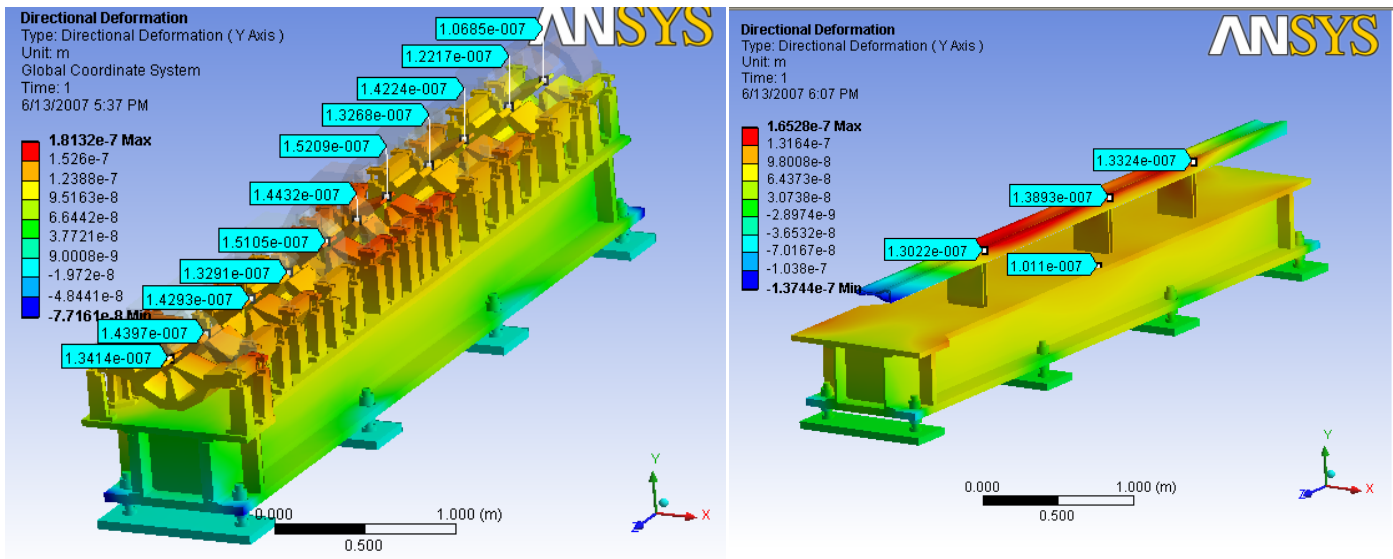


Figure 5.4: (a) Maximum vertical mis-alignment between the magnets $< 0.03 \mu\text{m}$, (b) maximum vertical deflection for the vacuum chamber at the BPM locations $< 0.15 \mu\text{m}$.

Table 5.2. Thermal deflection of the magnet's center from finite element analysis

Vertical displacement of the magnet center (microns)	Misalignment wrt central magnet (microns)	(Misalignment) ²
0.1340	0.0100	0.0001
0.1440	0.0000	0.0000
0.1430	0.0010	0.0000
0.1330	0.0110	0.0001
0.1510	0.0070	0.0000
0.1440	0.0000	0.0000
0.1520	0.0080	0.0001
0.1330	0.0110	0.0001
0.1420	0.0020	0.0000
0.1220	0.0220	0.0005
0.1100	0.0340	0.0012
RMS vertical misalignment (microns)		0.0138

Fig.5.4 shows the vertical displacements for the girder, magnets and vacuum chamber assembly corresponding to the temperature distribution in these components shown in Fig. 5.3. As shown in Table 5.2, the FEA results indicate that the RMS vertical misalignment between the magnets is $0.014 \mu\text{m}$ which is less than the design tolerance of $0.025 \mu\text{m}$ mentioned in Sec. 5.1. For the vacuum chamber, at the points supported by the invar plates corresponding to the BPM locations, the maximum vertical displacements are about $0.14 \mu\text{m}$ which is 2 times lower than 10% of the vertical beam size.

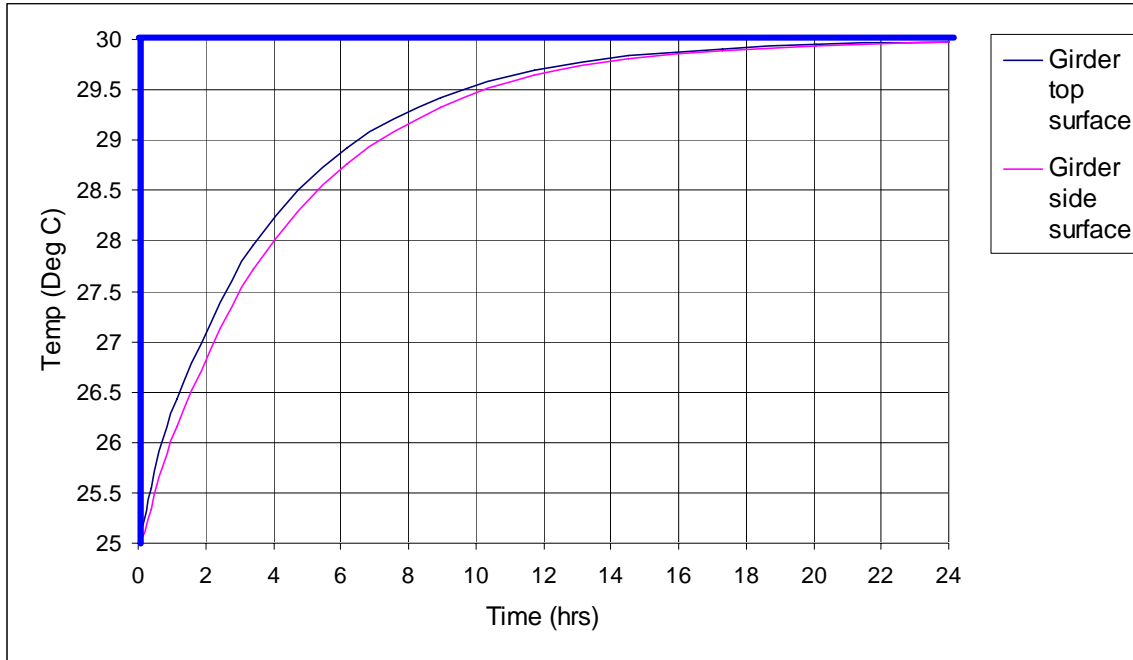


Figure 5.5: Time constant for the girder system

To compute the time constant for the girder assembly a step change of 5 °C in the tunnel air temperature was assumed. From the FEA analysis result shown in Fig.5.5, it can be seen that the temperature of the system reaches 29.9 °C in 24 hrs.

b) Vibration Stability

Sources that can induce mechanical vibrations in the girders magnets and vacuum chamber consist of turbulent flow in water cooling conduits and random ground motion. The effects of flow-induced vibrations can be minimized by paying close attention to several useful design guidelines, namely:

- 1) Locate all rotating equipment including fans, blowers, compressors, and pumps outside the storage ring tunnel, preferably tens of meters away from the tunnel flow and ceiling.
- 2) Keep low flow velocities (less than 2m/s) in the process water headers.
- 3) Design header supports to minimize their vibration, such as by integrating viscoelastic dampers in the headers hangers, or by attaching headers directly to the ceiling.
- 4) Arrange water flow circuits and connection fittings such that sharp bends are eliminated. Special attention is to be given to the routing and clamping of the hoses and tubes that connect the magnets and vacuum chambers to their respective headers.

There are several sources of random ground motion, such as compressors, rotating machinery, traffic and other “cultural noises”. Fig. 5.6 shows a comparison between the PSDs of the random ground motions near the NSLS-II site at the CFN building, at an NSLS beamline and at free field between NSLS and CFN.

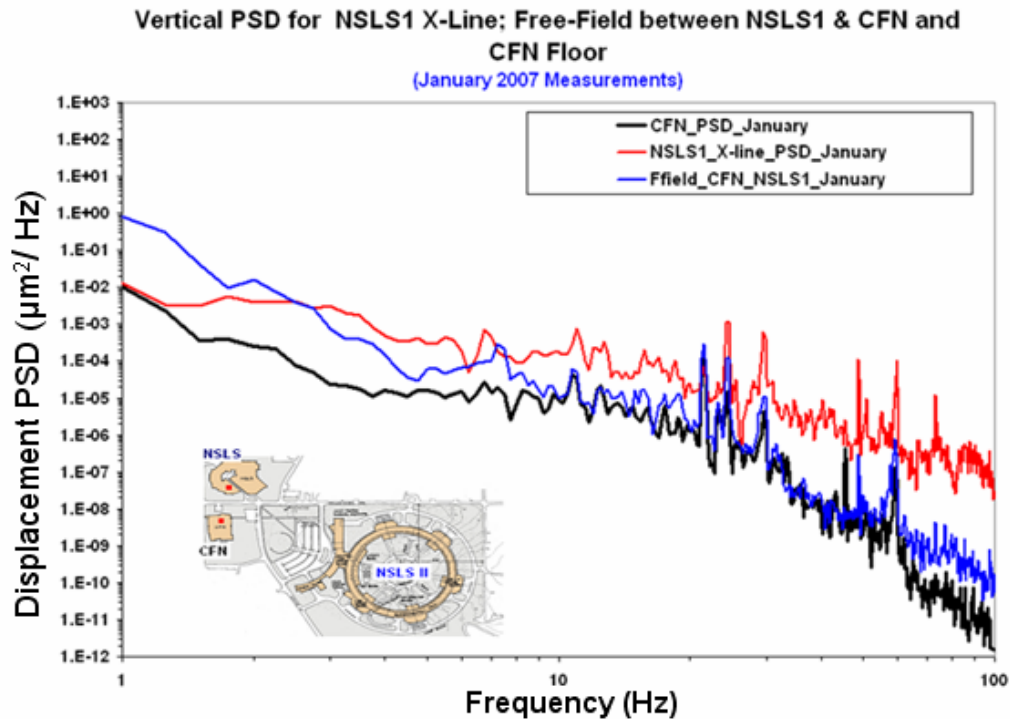


Figure 5.6: Displacement PSDs near the NSLS-II site [Ref. 5.4].

These PSDs compare favorably with those obtained at most of the light sources except for three peaks between 20-30 Hz from local noise sources. The RMS displacement at the CFN floor is approximately 20 nm (2-50 Hz), which indicates that the NSLS-II floor specification of 25 nm (4-50 Hz) is easily achievable. As expected, the ambient ground motion drops off sharply with frequency. There is considerable ground motion in the low frequency range, for instance, approximately 200 nm RMS in 0.5-4 Hz band. However, the floor motion of the storage ring in this low frequency range is expected to be highly correlated since the wavelength of the Rayleigh waves in concrete is greater than 600 m for frequencies lower than 4 Hz. Relaxed tolerances (yet to be specified) for such correlated motions are expected to be easily met with the use of real-time orbit feedback system. For frequencies greater than 30 Hz the RMS ground motion is 1 nm RMS in 30-100 Hz and hence will not have a significant effect on beam stability even if it is amplified by the girder assembly. Thus, the design goal for the girder support system is to have its first lowest natural frequency of greater than 30 Hz.

Finite element modal analysis of the NSLS-II girder and magnets assembly shows that the lowest two natural frequencies of the system are 54 Hz and 66 Hz. The corresponding mode shapes, rolling and twisting of the girder, are depicted in Fig. 5.7.

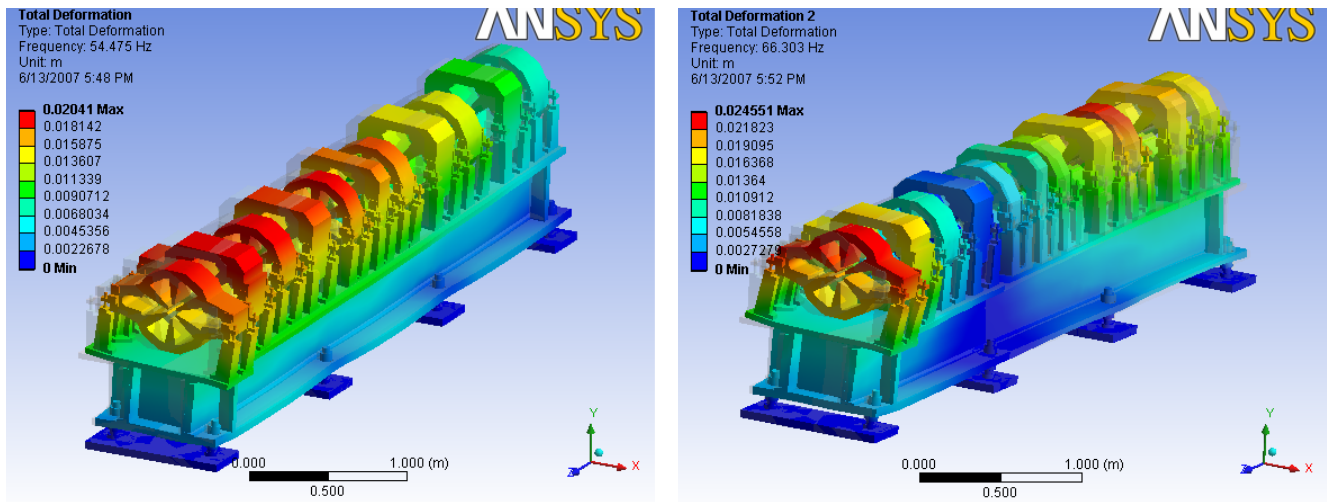


Figure 5.7: Natural modes of vibration for the girder-magnets assembly: (a) rolling mode = 54 Hz, (b) twisting mode = 66 Hz

Based on studies performed at the BNL site, it is expected that the relative settlement of the soil supporting NSLS-II would be 10 $\mu\text{m}/10 \text{ m}/\text{year}$. To investigate the effect of ground settlement on the girder stability, a displacement boundary condition of 20 μm was applied to the concrete slab under the extreme ends of the girder as shown in Fig.5.8. The FEA results show that the von Mises stress in the bolt are about 2 MPa which reduces to about 0.1 MPa at the interface between the concrete and the epoxy grout. Since the tensile strength of concrete is in the range of 2-5 MPa (300-700 Psi), a ground settlement of 20 microns will not cause cracks in the concrete.

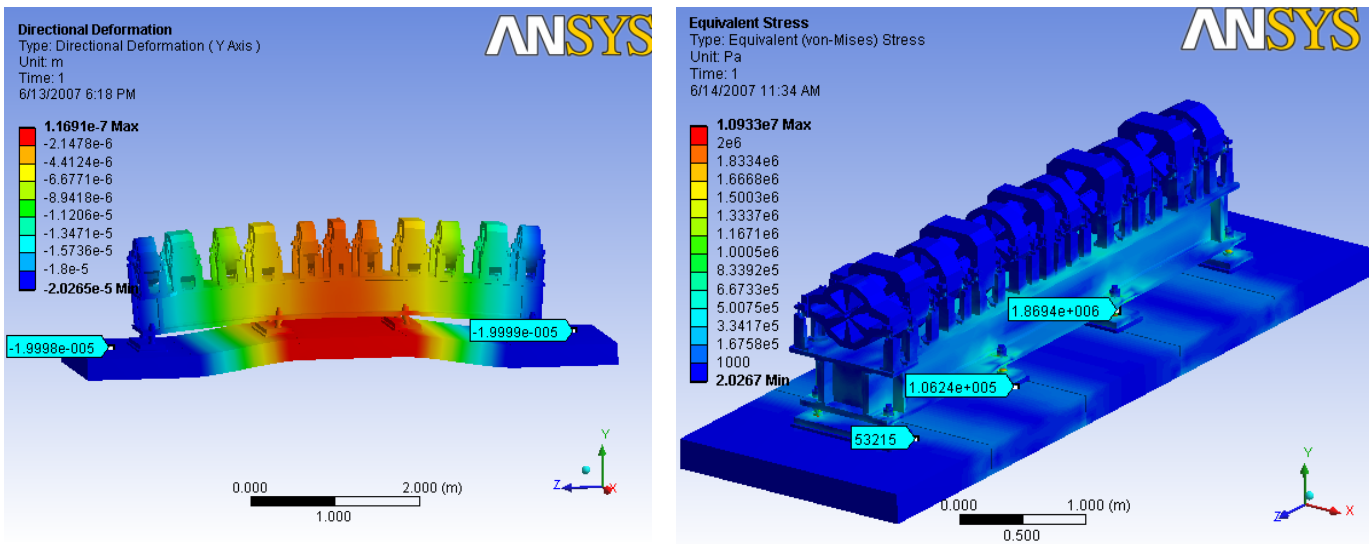


Figure 5.8: Effect of ground settlement on girder stability: (a) Vertical displacement contour plot, (b) von Mises stress contour plot

5.4. Mechanical Stability of User BPMs and X-BPMs

BPMs at the two ends of the insertions devices (user BPMs) and X-BPMS in the front ends have more stringent mechanical stability requirements. The vertical and horizontal RMS displacements are specified to be less than $0.1 \mu\text{m}$ and $1 \mu\text{m}$, respectively. We have investigated BPM support stands made from carbon fiber composites to meet the tight tolerance in the vertical direction. A carbon fiber composite can have thermal coefficient of expansion as low as $0.2 \mu\text{m}/\text{m}/^\circ\text{C}$. With the tunnel air temperature fluctuations controlled to within $\pm 0.1 \text{ }^\circ\text{C}$, the vertical displacement of 1 m high support stand can be maintained to about $\pm 0.02 \mu\text{m}$. The carbon fiber composites are, however, weak in the transverse (thickness) direction which can result in a system with very low natural frequency. Typical Young's moduli along the principal and transverse directions are 120 GPa and 7.5 GPa, respectively. From our preliminary discussions with vendors, we have been assured that the vendors can supply us with a 10-inch diameter carbon fiber composite that will meet the thermal design specification ($< 0.1 \mu\text{m}$) and natural frequency requirement ($> 30 \text{ Hz}$).

The second design option that we have investigated for the BPM support stands consists of a system of aluminum tube sandwiched between two structural steel tubes. A schematic of this design is shown in Fig. 5.9. In this design, the aluminum member counteracts the expansion of the steel members, and by carefully adjusting the lengths and diameter of each member it is possible to get zero thermal deflection at the BPM support point as indicated by the FEA thermal results (vertical displacement = $0.005 \mu\text{m}$) shown in Fig. 5.10.

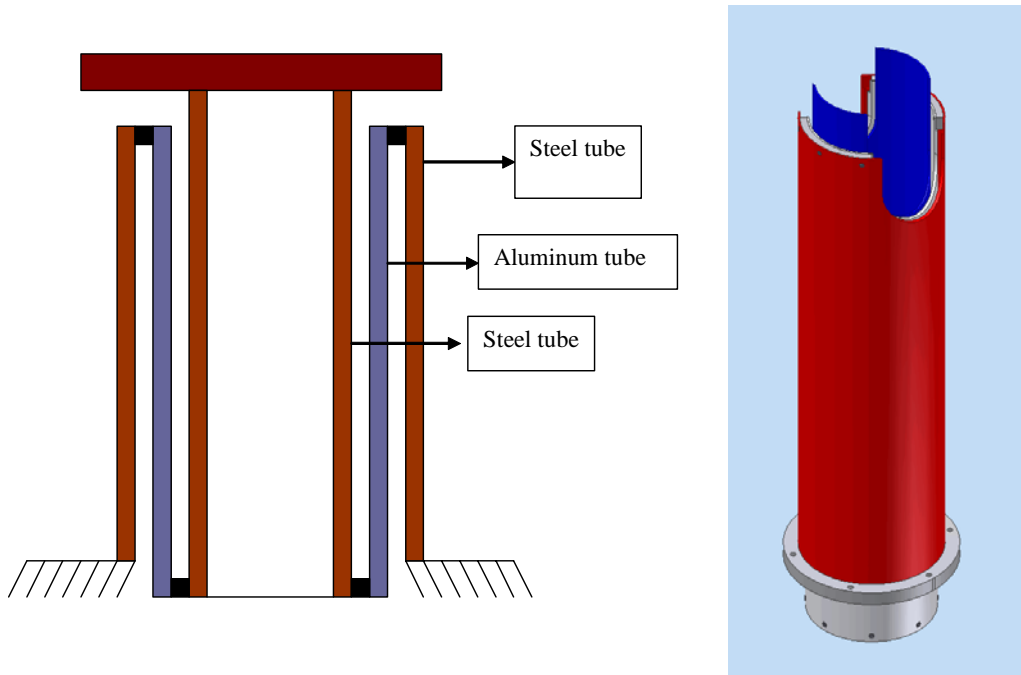


Figure 5.9: User BPM supports

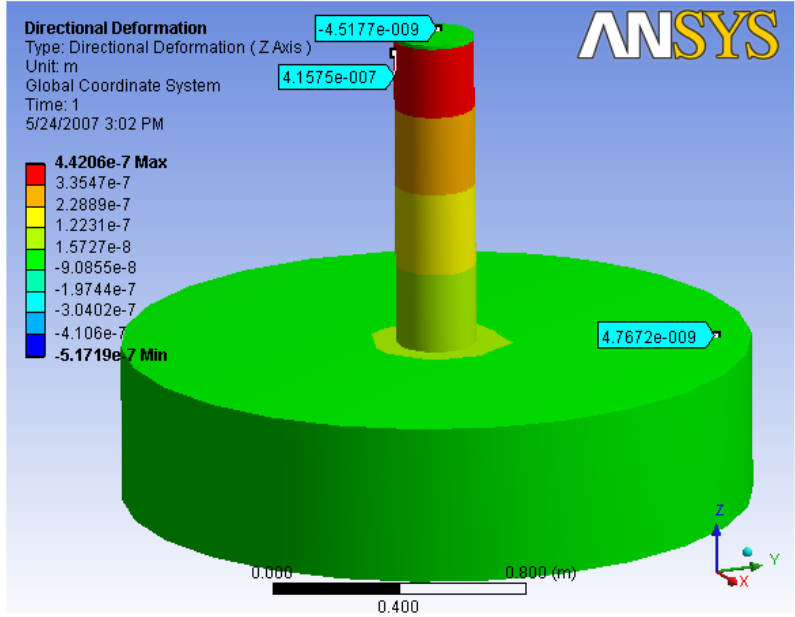


Figure 5.10: Maximum thermal deflection at user BPM support point = -0.0045 microns

Vibration FEA analysis results for this design are shown in Fig. 5.11. The lowest natural frequency for the system is 45 Hz which corresponds to vibration (swaying) in the horizontal direction. The RMS horizontal displacement (2-50 Hz, 1σ) is calculated to be 0.026 μm as compared to the specification of 1 μm .

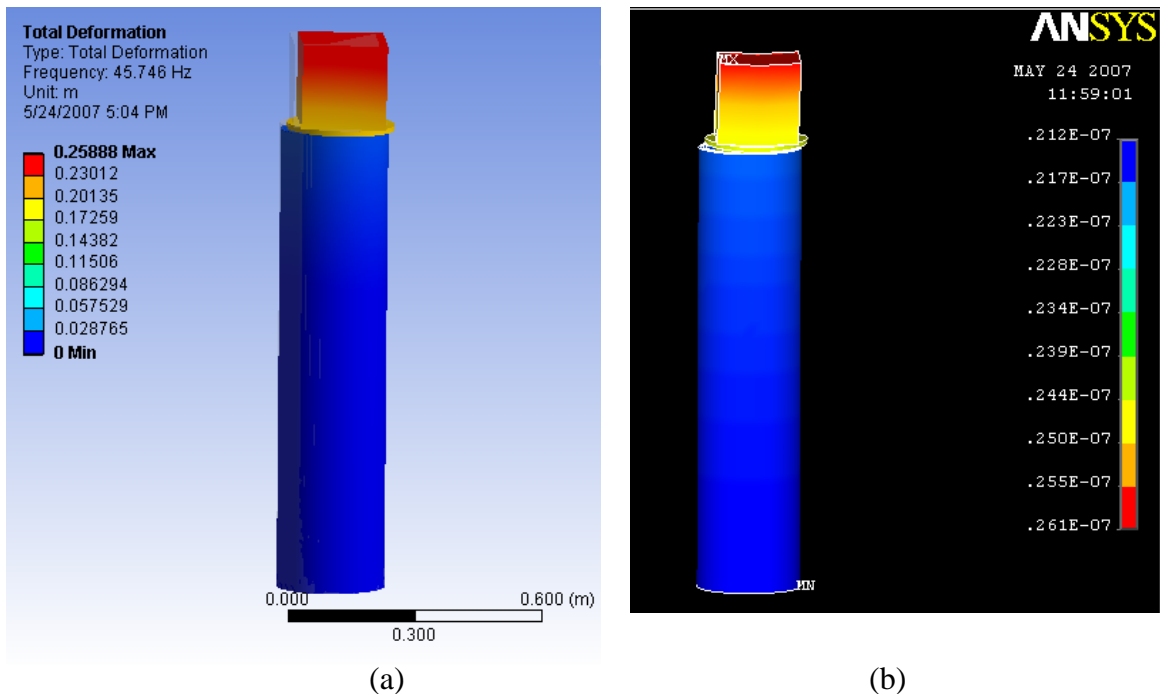


Figure 5.11: (a) FE model of a carbon fiber composite support stand, (b) displacement PSDs of base (blue curve) and BPM assembly (magenta curve).

5.5 Envisioned R&D on Mechanical Systems

Ongoing Tasks:

1. Design, analysis and fabrication of a prototype girder, vacuum chamber, chamber supports, and user-BPMs supports.
2. Magnet alignment using a vibrating wire technique. This includes estimating alignment errors due to tightening of the bolts.

Future R&D Tasks:

1. Vibration and thermal tests on the girder-magnet-vacuum chamber assembly.
2. Vibration and thermal tests on the user-BPM assembly.
3. Active vibration control for nanoprobe devices.
4. CFD simulations to establish air-flow patterns.

References

- [Ref.5.1] R.O.Hettel, "Beam Stability at Light Sources," *Review of Scientific Instruments*, 73, March 2002, pp.1396-1401
- [Ref.5.2] D.J. Wang, H.C.Ho, C.K. Kuan and J.R. Chen, "Experimental Study of Thermal Deformation of the Magnet Girder at SRRC Storage Ring," *Proceeding of APAC 2001, Beijing, China, 2001.*
- [Ref.5.3] J.R. Chen, D.J. Wang, Z.D. Tsai, C.K. Kuan, S.C. Ho, J.C. Chang, "Mechanical Stability Studies at the Taiwan Light Source," *MEDSI 2002, APS, Argonne ,IL, Sept.5-6, 2002.*
- [Ref.5.4] Verbal communication with N. Simos, Experimental ground motion data measured by N. Simos at various BNL locations.

6. Orbit Feedback

To realize the benefits of the high brightness and small beam sizes of NSLS-II, it is essential that the photon beams are exceedingly stable in position and angle. We shall require beam motion of no more than 10% of beamsize or angular spread. Ideally, the spatial and angular stability of the electron beam should be maintained for at least the duration of spectral scans, which typically run from a few ms to a few hours. Since the minimum vertical beta function is about 1 m, when we take the vertical emittance as $0.1\text{nm}/4\pi$, the vertical beamsize is $2.7\ \mu\text{m}$ rms. Therefore, we require the beam position stability to be $\sim 0.3\ \mu\text{m}$ in the short straight sections.

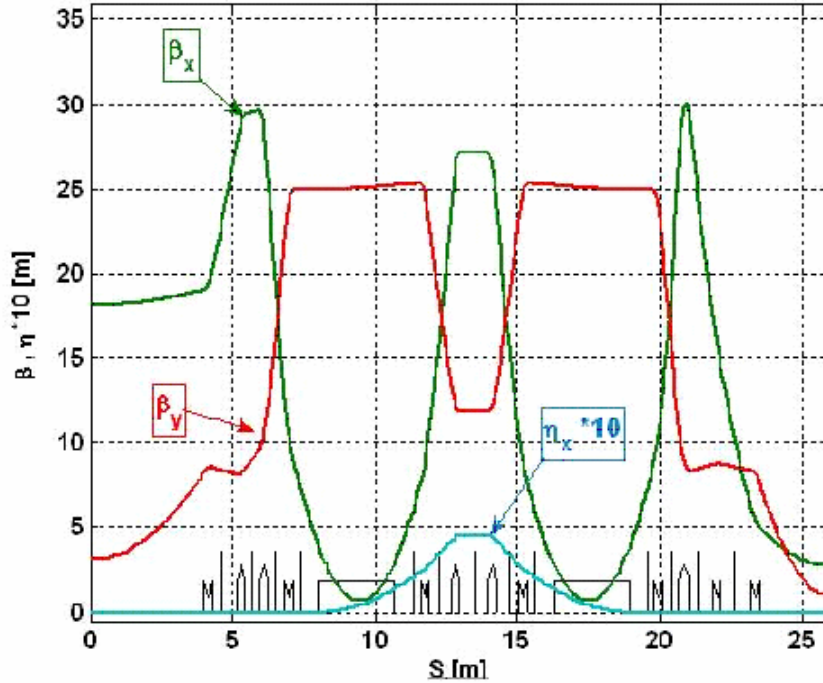


Figure 6.1: Lattice functions for one-half superperiod of DBA-30 lattice as specified in the CDR.

The lattice functions for the NSLS-II storage ring design as presented in the Conceptual Design Report (December 2007) are shown in Figure 6.1. For this lattice, we have calculated the performance of a fast, closed-orbit feedback system with 120 BPMs and 120 correction trims. To illustrate the system performance, we translated the quadrupoles randomly and independently according to a distribution with $1\ \mu\text{m}$ rms and also varied the transverse position of the BPMs by $1\ \mu\text{m}$ rms. We then averaged over an ensemble of 400 such configurations of random displacements. The resulting beam rms motion $\sigma_{\Delta y}$ is shown in blue in Figure 6.2. We see that it is well-approximated by the function $14\sqrt{\beta_y[m]}\mu\text{m}$, which is shown in green.

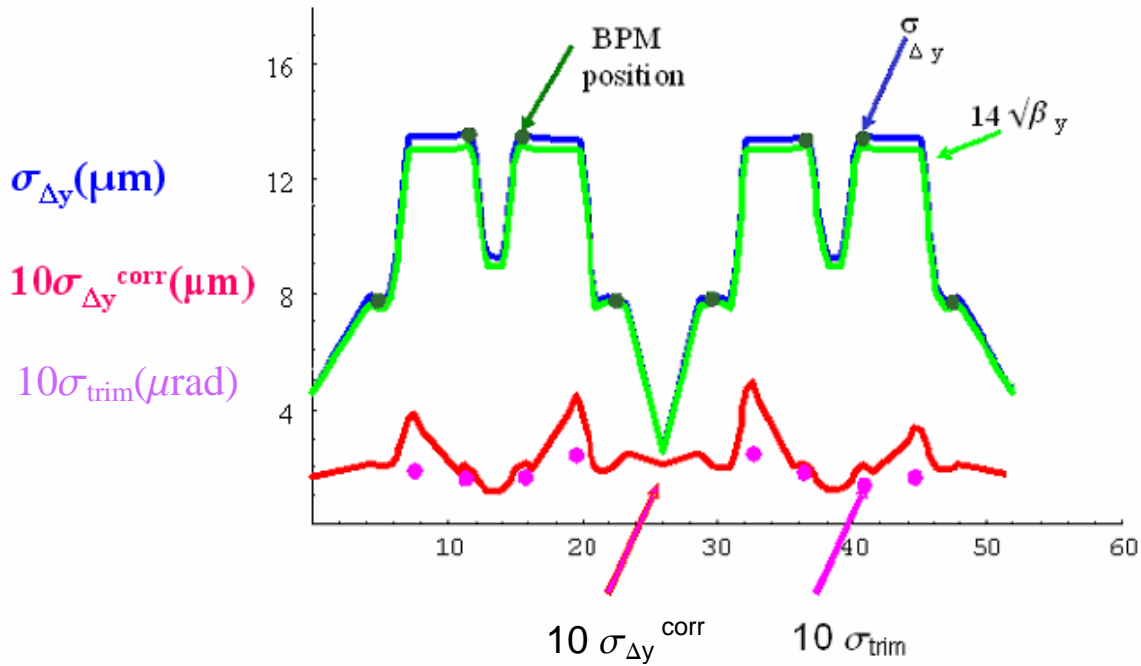


Figure 6.2: Illustration of feedback system performance correcting the orbit resulting from $0.2 \mu m$ rms random displacement of the quadrupoles and BPMs. The orbit correction uses 4 BPMs and 4 trim dipole correctors. The blue curve shows the uncorrected orbit and the red curve is 10 times the corrected orbit. The purple dots indicate ten times the strength of the correction magnets in μrad .

As an illustration, we considered independent Gaussian random errors for the quadrupole and BPM vertical vibration with rms displacement of $0.2 \mu m$. We calculated the open-loop BPM signal, then used the single-value-decomposition (SVD) matrix to calculate the corrector strength, and finally calculated the corrected orbit. After averaging over 400 random samples, we obtained the residual rms beam motion. From these results we can easily scale to deduce the behavior for any assumed rms displacement of the quadrupoles and BPMs. For example, if the rms quadrupole and BPM displacement was $0.1 \mu m$, then the orbit deviation and corrector strength would be reduced by a factor of 2.

In Fig. 6.2, to allow the residual orbit after correction (red curve) to be seen, we multiplied it by a factor of 10. The height of the purple dots represents 10 times the rms strength of the correctors, in units of μrad . The figure shows that the correction reduces the beam motion at the center of the short straight section ($z \sim 26m$) by a factor of ~ 10 , from $\sim 2 \mu m$ down to $\sim 0.2 \mu m$. The maximum RMS corrector strength is on the order of $0.2 \mu rad$. We conclude from these calculations that a feedback system utilizing 4 correctors and 4 BPMs can reduce the orbit motion sufficiently to meet our goals. We expect the vertical motion of the quadrupoles and BPMs to be on the order of $0.025 \mu m$ in the frequency range 4-50 Hz and $0.2 \mu m$ in the frequency range 0.5-4 Hz.

The beam motion due to power supply noise in a digital feedback system is determined by the voltage corresponding to the last bit of the power supply and the power supply current

noise itself. We find that if we require beam motion at the beam waist where $\beta_y = 1$ m to be less than $0.3 \mu\text{m}$, the RMS trim noise should be less than 10 n-rad. The specification for the corrector magnet power supplies is to provide better than $0.01 \mu\text{rad}$ resolution of the last bit and a noise level below $0.003 \mu\text{rad}$.

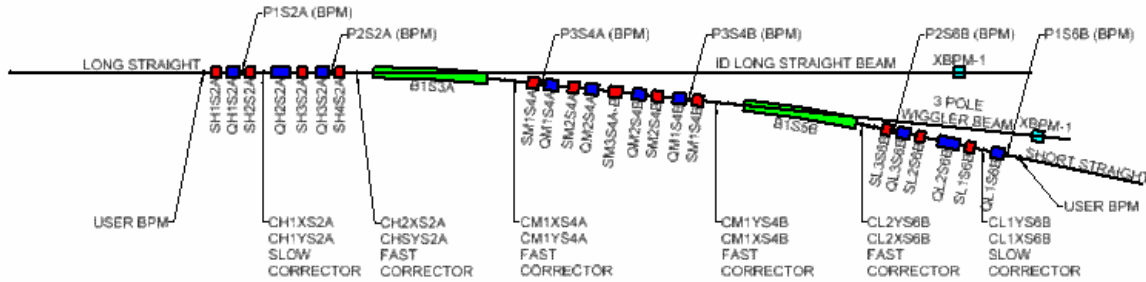


Figure 6.3: Schematic showing the position of the correction dipoles and the BPMs in one-half superperiod. This is the current lattice updated from that discussed in the CDR. In particular, the position for three-pole wigglers in the dispersive region is shown.

The quadrupoles and sextupoles will be aligned on girders to better than $50 \mu\text{m}$, and girders will be aligned relative to each other to better than $100 \mu\text{m}$. Beam based alignment will be used to calibrate the BPMs relative to the quadrupoles and sextupoles. The orbit correction system contains 7 correction magnets and 7 BPMs per half-superperiod as illustrated in Fig. 6.3. It has the capability of correcting the misalignment expected during first commissioning of the storage ring as well as for the long-term settlement of the concrete floor.

A subset of 4 correction magnets located over stainless steel bellows (to reduce eddy current effects) will be used in the feedback system. Use of 4 BPMs appears to be sufficient but we have the capability of using more than 4 if future considerations indicate that this is desirable. User BPMs on carbon-composite supports will be installed in straights having insertion devices, to provide the highest degree of thermal stability of the BPM position. We plan to incorporate x-ray BPMs located on the experimental beamlines into the orbit feedback system in order to improve angular stability. Only x-ray BPMs located before any optical elements will be fed back to the electron beam. X-ray BPMs located after optical elements can be used for feedback control of hardware in the experimental end-station. At this time we do not plan on using local feedback systems; however this option is not precluded if it is found to be beneficial.

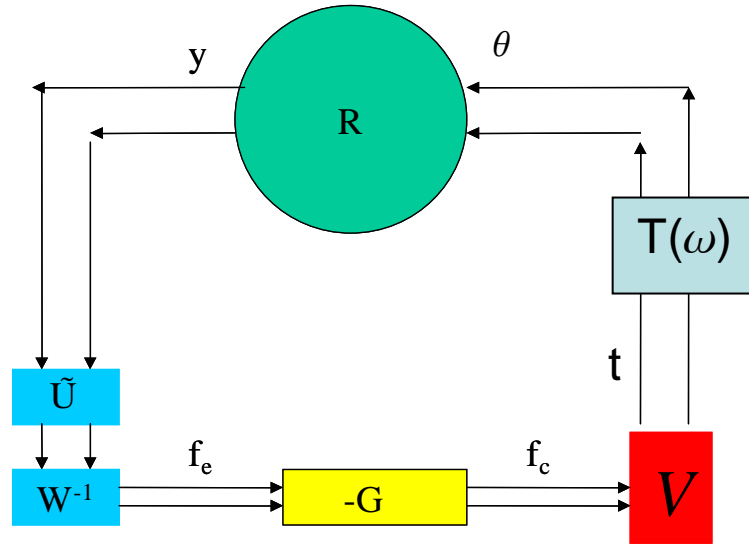


Figure 6.4: Schematic of the closed orbit feedback system based on single value decomposition of the response matrix.

A schematic of the orbit feedback system is presented in Fig.6.4. The response matrix R , between the corrector excitation and the orbit displacement at the BPMs, can always be decomposed in the form $R = UV\tilde{W}$, such that W is diagonal. Each eigenvector corresponds to an independent channel. The negative feedback gain G and the frequency response $T(\omega)$ are also diagonal. U and V are orthogonal with orthonormal columns (not necessarily square matrices). G is chosen to be large and positive and at low frequency the error signal is reduced by $1+G$. At higher frequency $T(\omega)G$ is complex and the system has to be carefully designed to avoid oscillation. In this regard, it is very important that all the correction magnets (including the effects of eddy currents in the chamber) have the same frequency dependence.

7. Electrical Systems

7.1 Global Beam Position system

A simplified block diagram of the global beam position system is in Fig. 7.1. The BPM requirements will be discussed in the instrumentation section. The planned system will have all BPM data transferred to a single process where the corrector strengths will be calculated. The corrector strengths will then be transferred to the individual power supply interface. Both slow/alignment and fast corrections will be calculated in this process. The global timing system will supply synchronized triggers for the system. The overall throughput of the system is ~ 5 kHz.

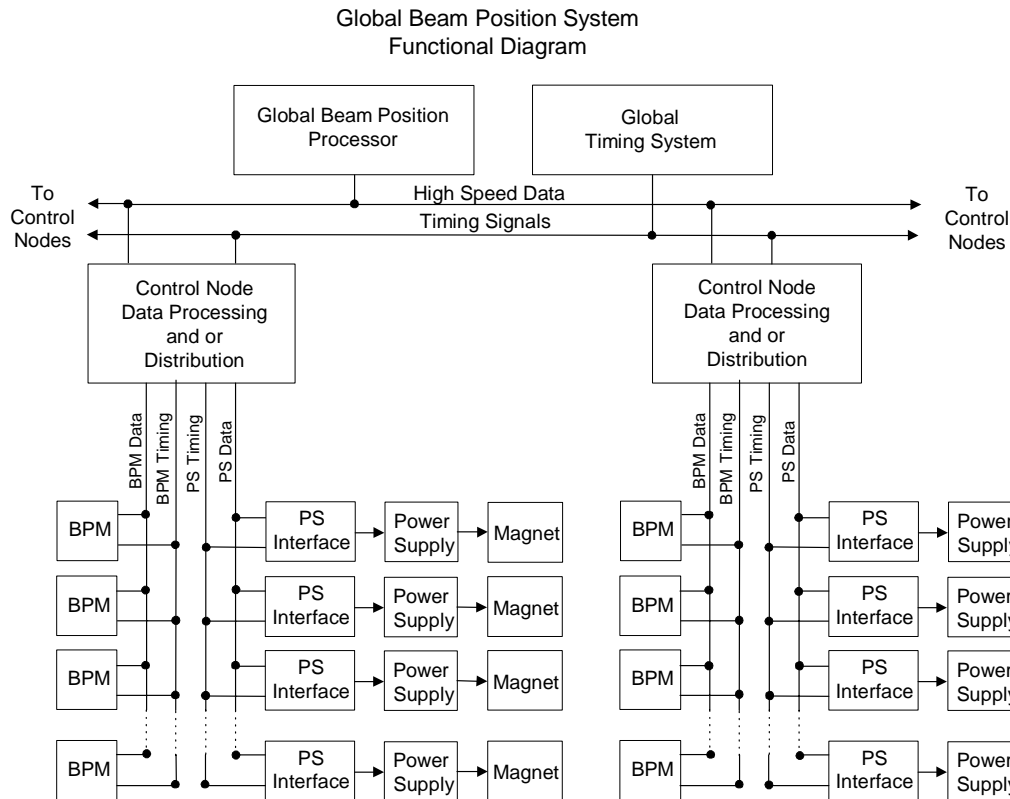


Figure 7.1: Block diagram of global position system

A more detailed design of the system needs to be done. Some critical items that need to be investigated are the following:

1. The methods of data transfer between the various elements of the system.
2. The number of bpm and ps interfaces that are connected to a control node.
3. The data throughput of the overall system.
4. The choice of the process platform that meets calculation speed requirements.

7.2 Corrector magnets and power supplies used for global beam position system

The feedback system will use 120 corrector magnets with separate horizontal and vertical coils. The magnets will be designed for fast correction of ~ 100 Hz. The dc transfer function of the magnet is $1000 \mu\text{rad}$ per 19.2 Amps. The magnets will be located over stainless steel bellows and

or flanges. This is to minimize the affect of eddy currents of low resistance beam chambers, like aluminum that will decrease the effective bandwidth of the system. The magnets are placed at the ends of each main dipole magnet. There will be 120 horizontal and 120 vertical power supplies. These corrector magnets and power supplies will be also used in slow and alignment corrections. The power supplies will have a high current requirement for slow/alignment corrections and high voltage requirements for fast corrections.

The power supply requirements from accelerator physics are the following:

Frequency	Strength - RMS
< 5 Hz	800 μ rad
20 Hz	100 μ rad
100 Hz	10 μ rad
1000 Hz	1 μ rad

Resolution of last bit: 0.01 μ rad
 Noise Level : 0.003 urad (~ 4 ppm of 800 μ rad)

These rating are for vertical correction and the horizontal correction is less stringent and they need to be quantified.

The present plan for the corrector magnets power supplies are to use a four quadrant switch-mode class D amplifier. This will be able to meet the high current and high voltage requirement in an efficient topology. The amplifier will be incorporated into a bipolar current regulated power supply. The small signal bandwidth of the power supply will be ~ 2 kHz. A possible problem with this power supply will be from current ripple from the switching frequency. The plan is to use an amplifier that has a switching frequency of 81 Hz. which should give a small ripple current of ~ 2 ppm.

The plot in Fig. 7.2 is the maximum fast correction strength of the power supply before it is limited by its maximum voltage or current.

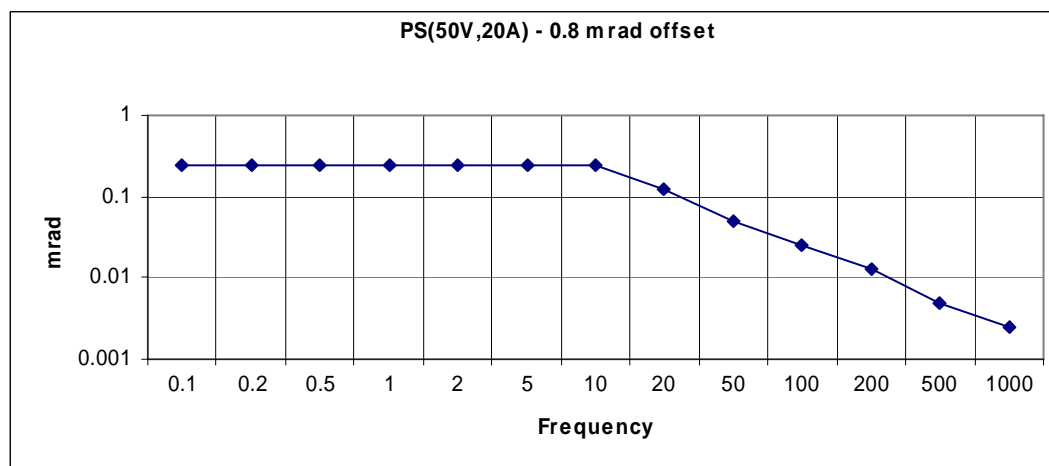


Figure 7.2: Peak corrector strength as a function of frequency for a corrector at a fixed offset of 800 μ rad for a bipolar power supply with a rating of 50 volts and 20 amps.

It is planned to use two 16 bit DACs in the power supply interface. The output of the DACs will be summed at different gains. The gain difference will be 16 which will give an effective resolution of 20 bits or $\sim 0.0008 \mu\text{rad}$. The high effective resolution is to minimize quantization noise in the overall system.

The following is the planned R&D for corrector power supplies and magnets:

1. Measure the magnet field of a proto-type corrector magnet as a function frequency. These measurements will include transfer function and multi-poles.
2. Design and build a proto-type corrector power supply measure short term stability and the frequency response of the current regulator.
3. Measure the current ripple of the power supply and overall current noise.

7.3 Power Supplies

(a) Main Dipole

The power supply is a unipolar, 2-quadrant, current-regulated supply. It will use two 12-pulse SCR converters in series with the center point connected to ground. This configuration will reduce the voltage to ground at the magnet load and reduce the voltage rating on various converter components. Each converter will have a two-stage LCRL passive filter and a series pass active filter. This is required to reduce the ripple current to low levels and minimize AC power line disturbances from the NSLS II and AGS boosters.

Each main dipole magnet bending angle is 0.1047 rad. The CDR has the current ripple spec. (referred to I_{max}) of 5 ppm for freq. 60 Hz and greater. This gives a $\sim 524 \text{ nrad}$ noise in the horizontal direction. (Assuming all the ripple current goes into the field.) The current ripple estimate may be reduced when a more thorough electrical circuit model is made for the dipole power supply. Also transmission line effects will have to be calculated.

CDR has the following power supply parameters:

resolution of reference current	18 bit \pm 1LSB
stability (8 h-10 s) – referred to I_{max}	40 ppm
stability (10s-300 ms) – referred to I_{max}	20 ppm
stability (300 ms- 0 ms) – referred to I_{max}	10 ppm
absolute accuracy – referred to I_{max}	100 ppm
reproducibility long term – referred to I_{max}	40 ppm

Redundant DCCTs will be used to confirm the power supply current reproducibility. High-precision DMMs and scanners will be used to monitor the power supply current, a redundant current sensor, and the analog current set point. This equipment will ensure long-term stability and reproducibility. The dipole cables will be installed with a twist to prevent pickup from the booster circuits or other noise sources.

(b) Multipole (Quad. & Sext.)

These circuits will use one power supply for each magnet. The power supply is a unipolar, single-quadrant, current-regulated switch-mode design. The power section is a commercial voltage-

controlled switch-mode programmable power supply with high output bandwidth (~ 1 kHz). The power supply will use a DCCT as the current feedback device. To minimize current ripple, an additional output filter will be used. The CDR has the current ripple spec. (referred to I_{max}) of 15 ppm for freq. 60 Hz and greater.

CDR has the following:

resolution of reference current	16 bit \pm 1LSB
stability (8 h-10 s) – referred to I_{max}	100 ppm
stability (10s-300 ms) – referred to I_{max}	100 ppm
stability (300 ms- 0 ms) – referred to I_{max}	100 ppm
absolute accuracy – referred to I_{max}	100 ppm
reproducibility long term – referred to I_{max}	100 ppm

Like the main dipole redundant DCCTs will be used to confirm the power supply current reproducibility. High-precision DMMs and scanners will be used to monitor the power supply current, a redundant current sensor, and the analog current set point. This equipment will ensure long-term stability and reproducibility.

Power supply output cables will be arranged to minimize pickup from other circuits. All power cables will be separated from signal cables.

The R&D for the multipole power supplies is to build a proto-type and confirm the accuracy, stability, and current ripple of the power supply.

7.4 Beam Position Monitors

Libera Electron utilizes digital signal processing and enables accurate beam position monitoring, trouble-free commissioning, and local and global feedback building. When input signal levels are from around -35 dBm to 0 dBm the resolution is constant due to prevailing influence of phase noise. For the BPM buttons located on the 25 mm radius the r.m.s. uncertainty in 1 kHz bandwidth of beam position is around 0.5 microns. The processing module is expected to have 2.5 microns 8-hour stability (with ambient temperature variation below 1°C), and temperature drift is expected to be 0.5 μ /°C.

With fast serial links, powerful FPGA and embedded CPU Libera Electron provides basis for orbit feedback building, with control system integration moved from the driver/backplane level to the network and transport layers.

As a result of mechanical, thermal and electronic drifts high pointing stability of the SR beam will be hard if possible to achieve utilizing only RF BPMs, which are located very close to the source point. Utilizing photon BPMs placed in the user beamline at significant distance allows to achieve the beam stability goals. Regular photon BPMs are based on measuring of the photocurrent from the blades made of refractory material and intercepting part of the photon flux from the insertion device or bending magnet. As it was demonstrated at APS with such BPMs it is possible to reach sub-microradian pointing stability, but at the expense of utilizing feedforward look-up tables to subtract predetermined offsets from the photon BPM readings as the ID gap varies. However, elevated noise/signal ration prevents using blades with large gaps. To overcome drawbacks pertinent to photoemissive photon BPM is was suggested by G. Decker et al. to employ back

fluorescent BPMs. The horizontal fringes of the photon beam strike the copper target, which re-radiates fluorescent photons of approximately 8 keV energy. A set of four p-i-n diode detectors located above and below midplane then detect the fluorescence. Such BPMs are less sensitive to the stray synchrotron radiation from the elements of the ring and demonstrated high stability when intensity of the photon beam varied by factor of million. Such devices will be considered for utilization as well.

7.5 Envisioned R&D for Power Supplies

The planned R&D is as follows.

Correcter PS & Magnet:

1. Measure the magnet field of a proto-type corrector magnet as a function frequency. These measurements will include transfer function and multi-poles.
2. Design and build a proto-type corrector power supply, measure short term stability and the frequency response of the current regulator.
3. Measure the current ripple of the power supply and overall current noise.

Main Dipole PS & Magnet:

1. Measure the magnet field of a proto-type dipole magnet (short proto-type). These measurements will include transfer function and multi-poles.
2. Start circuit modeling of main dipole ps circuits.
3. Design and build a proto-type series pass active filter.

Multipole PS & Magnets:

1. Design and build a proto-type and confirm the accuracy, stability, and current ripple of the power supply.
2. Design and build a temperature controlled enclosure. Confirm the effectiveness of the chilled water to air heat exchanger.
3. Measure the magnet field of a proto-type magnets (when available). These measurements will include transfer function and multi-poles.

8. RF System

The electron beam longitudinal phase space is determined by the RF cavity fields and the interaction of the electron beam with impedances in the ring. Jitter in the RF cavity fields can cause energy or phase jitter of the electron beam. This can transform into transverse beam size or jitter by increasing the effective emittance and through dispersion.

The electron beam can interact with impedances in the ring causing intra and coupled bunch energy and phase oscillations leading to emittance dilution and transverse beam motion through dispersion. Reliability of the RF system and the accelerator in general can be thought of as a low frequency limit of beam stability. Choice of hardware approach and design can have large effects in the reliability of the machine. This report will concentrate primarily on the effects of jitter in the RF fields causing electron beam motion and in turn jitter in the photon beam, in the bandwidth of sub-hertz (primarily thermal effects) to tens of kilohertz. In the following sections tolerances on the phase and amplitude jitter will be derived from user requirements and causes of RF system amplitude and phase noise will be described.

8.1 RF tolerances imposed by user experiments

Timing experiments, such as pump probe experiments, require that the timing jitter of the bunch be less than 5% of the RMS bunch length over the frequency range of 500 Hz to 50 kHz. This corresponds to a phase error of 0.1 degree for a 10 ps bunch, or a corresponding momentum jitter of 0.005% due to synchrotron motion.

The majority of users are not concerned with timing experiments but require small and stable photon beam size. The vertical photon beam divergence for an experiment using a higher harmonic of an Insertion Device (ID) is given by¹

$$\sigma_{y'}^2 = \frac{\lambda_n}{2L} \sqrt{1 + 16n^2 N^2 \sigma_\delta^2} + \frac{\epsilon_y}{\beta_y} \quad (1)$$

Where n is the harmonic of the ID being used, N the number of periods, L the length of the ID, σ_δ the momentum deviation, ϵ_y the vertical emittance of the electron beam and β_y the vertical beta function of the lattice at the insertion device location.

For NSLS-II $\epsilon_y \sim 8 \times 10^{-3}$ nm·Rad and $\beta_y \sim 1$ m at the ID straights, $L \sim 3$ m, $N \sim 100$. Because of the n^2 dependence, the worst case is for $n \gg 3$ where the two terms on the right hand side of equation (1) are comparable. Thus using (1) for a 10 % increase in beam size the momentum jitter must be 40% of the inherent momentum spread, or equivalently a phase jitter of 1.2 degrees.

A third limit on momentum spread is due to longitudinal energy oscillation leading to filamentation and increase in beam size. With a momentum kick $\Delta p/p$ to the bunch, an electron would have a longitudinal oscillation

$$\delta(t) = (\Delta p / p) \sin v_s \omega_0 t + \delta_0 \sin v_s \omega_0 (t + t_0).$$

Because of the longitudinal tune spread the two terms will decohere and become

$$\delta(t) = (\Delta p / p) \sin v_s \omega_0 (t + t_1) + \delta_0 \sin v_s \omega_0 (t + t_2)$$

where t_1 and t_2 are two random numbers. Averaging over t_1 , t_2 and δ_0 we arrive at

$$\sigma_\delta = \sqrt{\frac{1}{2} (\Delta p / p)^2 + \sigma_{\delta,0}^2} = \sqrt{1 + \frac{1}{2} f^2 \sigma_{\delta,0}^2}$$

where $f = (\Delta p/p)/\sigma_\delta$ is the relative kick factor. For a 10% increase in σ_δ , $f \sim 0.65$ or $\Delta p/p = 6.5 \times 10^{-4}$. The corresponding phase jitter is given by $\Delta\phi = \frac{h\alpha_c}{v_s}(\Delta p/p)$ where h is the harmonic number (1320), α_c is the momentum compaction factor = .00037 and $v_s \sim 0.01$, $\Delta\phi = 1.8$ degrees.

Another effect is due to the residual dispersion. As is mentioned earlier, the straight sections of NSLS-II are designed to be zero dispersion. However, due to lattice errors there will be residual dispersion. The order of magnitude is about 1 mm, same for the vertical and horizontal directions. The vertical beam size is much smaller; therefore, the limit will come from the vertical plane. In the vertical direction,

$$\sigma_y = \sqrt{(\epsilon_y \beta_y + \eta_y^2 \sigma_\delta^2)}$$

Because the second term in the square root is much less than the first term, the momentum spread change is not going to cause a notable change in the vertical beam size. However, the vertical position $y = y_0 + \eta_y \langle \delta \rangle$. The allowed centroid jitter is 10% of the beam size, or, $0.3 \mu\text{m}$; therefore the average momentum jitter should be less than 3×10^{-4} with a corresponding phase jitter limit of 0.82 degrees.

The beam size of some of the beam lines at the NSLS-II is dominated by the dispersion, such as the dipole beam lines and three-pole wiggler beam lines. For those beam lines, momentum jitter induces horizontal position jitter. The 10% rule requires the momentum jitter to be $\Delta p/p < 1 \times 10^{-4}$. The beam size is proportional to the momentum spread. From Eq. (4) and Eq. (5) we found the momentum oscillation should be less than 6.5×10^{-4} for long time measurements and 4.6×10^{-4} for the short time measurements. Consequently for these beam lines the tolerance is $\Delta p/p < 1 \times 10^{-4}$ which is from the position stability requirement. Many experiments have a stringent requirement on the horizontal angle stability. The minimum tolerance is about 1 μrad . Because the derivative of dispersion $\eta' \sim 0.1$, 1 μrad requires $\Delta p/p < 1 \times 10^{-5}$ which is too small to realize. These experiments would have to use the ID's in the zero dispersion straights. The above limits are summarized in Table 8.1.

Table 8.1: Longitudinal beam stability requirements

	Phase jitter $\Delta\phi$ ($^\circ$)	Momentum jitter ($\times 10^{-4}$)
Timing-dependent experiments	0.1	0.5
Vertical divergence (from momentum jitter)	1.2	4
10% increase in σ_δ due to filamentation	1.8	6.5
Vertical centroid jitter (due to residual dispersion)	0.82	3
Dipole Beam lines	0.27	1

Due in large part to the near zero dispersion in the ID straights which mitigates the effect of momentum jitter, the tolerance on the RF is dominated by the IR timing experiments.

8.2 System contributions to RF amplitude and phase noise

The RF system can contribute to beam jitter both actively and passively. Noise injected into the RF system anywhere in the signal path can be amplified and superimposed on the RF cavity fields. In particular, broadband “white” noise of the master oscillator can excite synchrotron oscillations in the beam causing beam motion. Studies² have shown that this can be exacerbated by the Robinson frequency shift which shifts the beam frequency response toward lower frequencies. Since the master oscillator phase noise falls off exponentially, the beam response function maxima shifts towards higher noise levels. In addition to oscillator noise the system is sensitive to power supply noise. One candidate high power klystron has a RF phase variation vs. DC power supply (anode) voltage of 12 degrees / %V. The modern pulse-switch-modulation (PSM) power supply has typical noise/ripple performance listed in table 2.

Table 8.2. THALES 54kV 12A PSM power supply

Typical noise/ripple performance	
Full range	< 1 % pk-pk
75 V (0.138%)	From 1 kHz – 2 kHz
15V	From 2 kHz - 4 kHz
3 V	From 4 kHz – 12 kHz
50 V	For > 12 kHz

If left uncorrected, the power supply ripple would contribute 1.6 degrees of phase jitter. Feedback either around the klystron directly or including the cavity can bring this to acceptable levels.

8.3 Collective effects

The beam can interact with fundamental and higher order mode impedances causing instabilities. Initial studies show the beam to be longitudinally stable in the presence of the 500 MHz cavity system. Further studies are required for the Landau cavity HOM's, whose 7k-ohm impedance would be unstable in the absence of the tune spread induced by the long bunches created by the combined 500MHz/1500MHz system. This bunch-lengthening cavity also induces a phase shift of the bunches along the bunch train comparable to or exceeding the bunch length³, although no problems have been identified by user experiments yet.

The bunch is unstable in the presence of the rings transverse broadband impedances, and NSLS-II will require a transverse damper.

A more comprehensive discussion of the collective effects is given in references [4,5]

- 1) Weiming Guo et al, “Longitudinal beam parameter tolerances of NSLS-II” PAC 2007
- 2) J. Byrd et al, “Effects of phase noise in heavily beam loaded storage rings” PAC 1999
- 3) N. Towne, Bunch and RF Stability and RF Noise in NSLS-II” NSLS-Tech-note #0027
- 4) S. Krinsky et al, “Collective effects in the NSLS-II storage ring” PAC 2007
- 5) NSLS-II Conceptual Design Report
<http://www.bnl.gov/nsls2/project/CDR/>